Reliability Engineering and System Safety 260 (2025) 111029

Contents lists available at ScienceDirect

Reliability Engineering and System Safety

journal homepage: www.elsevier.com/locate/ress

Methodological guidance and quantitative measures regarding seismic capacity and safety of freestanding and inelastic anchored nonstructural elements housed in ordinary and critical facilities

Danilo D'Angela [a], Gennaro Magliulo [a,b,*]

[a] Department of Structures for Engineering and Architecture (DIST), University of Naples Federico II (UNINA), Via Claudio 21, 80125, Naples, Italy
[b] Construction Technologies Institute (ITC), National Research Council (CNR), Viale Lombardia 49, 20098, Milano, Italy

ARTICLE INFO

Keywords:
Seismic capacity
Seismic safety
Nonstructural
Acceleration-sensitive elements
Rocking
Anchored equipment
Inelastic behavior

ABSTRACT

The study provides a comprehensive investigation of the seismic capacity and safety assessment of nonstructural elements (NEs). A general and extendable methodology is developed for robust assessment of two representative model categories of NEs: rocking-dominated rigid blocks (RBs) and inelastic single-degree-of-freedom (SDOF) systems, accounting for most acceleration-sensitive elements housed in ordinary and critical facilities. Numerical analysis is carried out implementing nonlinear dynamic models for NEs and accounting for multiple features, such as loading history types (ground and floor motions), NE dynamic properties, intensity measures (IMs), and multiple damage states (DSs). Quantitative capacity measures are provided, as well as novel closed-form equations are proposed for expeditious capacity assessment of NEs, including both capacity curves and surfaces. The seismic safety of the investigated NEs is estimated considering both ordinary and critical buildings, over low- to high-seismicity sites in Italy.

1. Introduction

1.1. Seismic safety

The seismic safety of nonstructural elements (NEs) is an issue of paramount importance for public safety and economy, as well as it represents a critical research issue in structural and earthquake engineering [1]; this is even more significant in case of strategic/critical buildings [2] and critical facilities [3]. The seismic safety associated with NEs can be assessed by comparing seismic capacity and demand measures, according to simple to complex methods. Several studies assessed the seismic capacity of various NEs by means of experimental tests [4,5] and analytical/numerical methods [6,7], as well as both regulations [8–10] and literature studies [11–13] provide methods and formulations for the estimation of the seismic demands on NEs.

Acceleration-sensitive NEs are a wide range of NEs that are sensitive to inertial effects but that can also be sensitive to applied (relative) deformations. Most NEs, excluding extremely complex and network systems, can be categorized as (a) freestanding/unanchored elements or (b) anchored elements [14]. The first category of elements can be often associated with a rigid-dominated response under seismic actions, which can be governed by rocking, sliding, or mixed mechanisms, mostly according to element geometry (shape and slenderness) and element to support interface properties [15,16]; these elements are typically modeled as rigid blocks (RBs) [17,18]. The second category can be typically referred to base-constraint structural schemes, where the base constraints consist in fastening or anchorage systems [5,19]; very often the seismic response of the abovementioned elements can be reasonably modeled by single-degree-of-freedom (SDOF) systems [11,20].

1.2. Freestanding elements

The dynamics of RBs was investigated since early times. In 1885, Milne [21] found that block overturning is associated with ground acceleration exceeding gravity acceleration constant; in 1927, Kirkpatrick [22] identified the significance of block size and ground motion duration on the dynamics response of rocking blocks; in 1960, Muto et al. [23] theorized the negative stiffness associated with the behavior of rocking blocks, also identifying the relevance of hyperbolic functions on

* Corresponding author at: Department of Structures for Engineering and Architecture (DIST), University of Naples Federico II (UNINA), Via Claudio 21, 80125, Naples, Italy.
E-mail address: gmagliul@unina.it (G. Magliulo).

https://doi.org/10.1016/j.ress.2025.111029
Received 15 July 2024; Received in revised form 4 February 2025; Accepted 13 March 2025
Available online 15 March 2025

the dynamics. The first systematic work on RBs (*classical theory*) is typically referred to the seminal study by Housner [24], who noted that expectedly unstable systems such as slender structures, "Golf-ball-on-a-tee" systems, and freestanding elements resisted to strong earthquakes, often without major damage, whereas relatively rigid structures and components suffered seismic damage. By theoretically investigating equilibrium and dynamics of RBs, Housner characterized the influence of the block size on the rocking stability, also referring to probabilistic metrics. Since Housner, researchers of the caliber of Priestley [25] and Chopra [26] studied the seismic response of RBs, and this topic is still a significant object of interest in current research. Most past studies on RB dynamics often addressed the theoretical and analytical aspects [16,18], focusing on the seismic response of geologic structures [27], ancient monuments [28,29], and museum objects [30,31]. In both literature and practice applications, rocking response was also meant as a seismic protection strategy for structures and infrastructures, given the negative stiffness (no resonance), the gravity recentering (if overturning does not occur), relatively typical large rotational inertia, and the possibility to provide the blocks with safety devices [32,33]. In some studies, rocking behavior was mitigated by developing active seismic protection techniques and technologies [34,35]. More recently, rigid and rocking-dominated response was investigated with regard to laboratory/technical equipment [36,37] and building contents [38,39].

Literature studies assessed the seismic capacity of rocking-dominated blocks and provided statistical models and closed-form expressions associated with ground-located [27,37,40] and building floor-located [38,39,41] components. Fragiadakis and Diamantopoulos [39] provided a simplified methodology to assess seismic fragility by processing building fragilities and RB dimension. D'Angela et al. [38] provided fragility parameters of building RBs accounting for a wide range of real building records and RB scenarios, referring to multiple DSs. Kazantzi et al. [41] developed analytical expressions for expeditious prediction of (building) floor-located RB response, referring to multiple RB building height locations. Despite researchers having been studying rocking dynamics for more than a century, the topic still motivates and inspires current researchers. Several research questions have not been responded to, and there is an urgent need to investigate further the issue, as is discussed in the following.

1.3. Anchored elements

The seismic assessment of anchored NEs is often carried out, especially in the practice, considering linear elastic response of NEs and implementing a spectral-based approach [11,13,42]. Very recent studies accounted for the nonlinear response of acceleration-sensitive NEs, implementing numerical/analytical methods and considering results from experimental tests. Tamura et al. [43] assessed the response of inelastic SDOF systems to model anchored equipment, considering constant-ductility floor spectra responses. They found that the yield strength of the investigated elements can be reduced due to the inelastic response of structure and SDOF element, and they proposed criteria for estimating the yield reduction factor as a function of SDOF vibration period, ductility factor, and stiffness ratio. Obando and Lopez-Garcia [44] investigated the seismic response of inelastic NEs under linear floor motion response of multistory buildings, accounting for an elastic-perfectly-plastic behavior of SDOF, modeled by a response modification factor. They characterized the SDOF inelastic displacement ratio response associated with multiple building scenarios, discussing the influence of the record type (floor/ground motion), also developing formulations for estimating the inelastic displacement ratios. Kazantzi et al. [45] investigated the influence of the nonlinearities on the strength of non-degrading SDOF systems with a bilinear hysteretic behavior, considering floor motions recorded in instrumented buildings. The study supplies an analytical formulation to estimate the strength reduction factor, useful for the assessment of seismic demands on anchored NEs. Elkadi et al. [46] proposed a new design methodology for NEs that accounts for the expected nonlinear behavior of the NE to structural connections, with a focus on strength and deformation demands. The methodology was derived from the results of an extended experimental campaign, accounting for several NE characteristics. Feinstein and Moehle [20] carried out experimental tests on shake table to assess the influence of NE attachment nonlinearities on the seismic response of NEs, considering a wide range of attachment properties; among the significant technical and scientific insights, the study stresses the need for improving current building codes by accounting for a more consistent design of NE attachments. Kazantzi et al. [47] recently investigated the seismic design of acceleration sensitive elements in industrial facilities, assessing and comparing the design options provided by the 2022 revised version of the new Eurocode 8 [48] characterizing the technical implications and the effects of the alternative design routes. Very recently, Vukobratović and Fajfar [49] developed closed-form formulations of floor acceleration spectra for nonlinear SDOF systems, which have been implemented in the current draft of the new Eurocode 8.

1.4. Limitations of current literature and research gap

Both categories of acceleration-sensitive NEs discussed above are often associated with an extremely high seismic risk, and there is an urgent need for further research investigations [50,51]. Regarding rocking-dominated elements, past studies often addressed specific case studies, more often structures, without considering a systematic approach, and rarely accounting for building response. Most studies investigating NEs implemented linear elastic assessment, and the very recent studies that accounted for the nonlinear response of acceleration-sensitive SDOF systems generally focused on developing technical criteria for estimations of seismic demands (floor spectra) and strength reduction factors, in the framework of design procedures, without addressing the capacity and safety assessment contexts. Furthermore, while the framework for NE seismic safety assessment has been addressed by very recent studies [51,52], and general approaches are defined within the relevant codes [9,10], no studies, to the authors' knowledge, provided methodological guidance for estimating seismic capacity and performing seismic safety assessment of NEs implementing simplified and expeditious methods, which are still relatively reliable and robust.

In the broader context of acceleration-sensitive NEs, the literature provides (a) technical methods for determining seismic capacity of some types of nonstructural elements and capacity models [7,38,39,41,47,53,54] and (b) technical methods and formulations for estimating seismic demands on nonstructural elements [11–13,49,55]; (c) very few studies provide seismic design principles and recommendations [47,56], as well as the draft of Eurocode 8 [48], as discussed in [47], report design methodology. However, some limitations of the literature/codes include but are not limited to the following ones: (a) developed/proposed capacity models/measures often (a1) refer to specific nonstructural element properties [39], (a2) are not easily generalizable and not directly applicable, as a methodology, to different element types/characteristics [20], (a3) often refer to linear elastic elements (for SDOF elements), (a4) do not provide both ground and floor engineering demand parameters or do not highlight the influence of the building on the capacity [41], (a5) do not provide closed-form correlations between statistical capacities, damage state (or performance level), and dynamic properties of nonstructural elements; (b) demand formulations and measures provided in the literature [13,49,55] do not clearly refer to specific performance levels and damage states, and are not explicated for ordinary or critical buildings; (c) seismic design procedures are proposed/reported [47,48] but safety assessment methodologies are not defined/developed or not referred to the context of potential applications in practice [57]; (d) seismic safety measures are not provided. No studies, to the authors' knowledge, (a) supply applicable quantitative safety measures associated with various NEs and (b) correlate, in a systematic and robust manner, the seismic response and safety of RBs

and SDOF systems to geometric/dynamic NE properties and representative site/building scenarios.

1.5. Aim and outline

The study aims to develop methodological guidance and quantitative measures associated with seismic capacity and safety of NEs. Seismic assessment of RBs and inelastic SDOF elements is implemented, attempting to push further the boundaries of knowledge by addressing the abovementioned research gaps, following the line of research that the authors have been investigating for the last years [13,38,54,58–64]. In particular, a systematic and comprehensive approach is defined implementing the same methodology and metrics for both NE categories, without particularizing the methods and the results and maximizing the comparison and critical evaluation efficiency. Both seismic capacity and safety associated with the abovementioned NEs are assessed, elaborating past data and developing new data; methodological guidance are provided, and quantitative safety metrics are estimated. Nonlinear dynamic analysis and damage assessment are carried out, accounting for both ground and floor motions as loading histories, also characterizing the influence of the main geometric and dynamic properties of the investigated NEs, considered to be housed in both ordinary and strategic/critical facilities, in low- to high-seismicity sites in Italy. A notation table is reported in the Appendix.

2. A comprehensive framework

2.1. Performance levels, limit states, damage states, and safety verification

Performance-based earthquake engineering (PBEE) assessment [65,66] and its implementation in codes [67,68] and literature [52,69] is based on multiple performance levels (PLs) and typically accounts for the following PLs [9,10]: immediate occupancy or operativity, damage limitation, life safety, and near collapse or collapse prevention. Limit state (LS) verifications represent the means to pursue the PL objectives. Immediate occupancy and damage limitation PLs are associated with serviceability LSs, i.e., operativity limit state (OLS) and damage limitation limit state (DLS), whereas life safety and near collapse PLs are related to ultimate LSs, i.e., life safety limit state (LSLS) and near collapse limit state (NCLS). The seismic safety assessment of structures and NEs is generally based on the comparison of capacity and demand measures associated with LS. The safety verification is performed according to assessment procedures that can be implemented through simple to complex methods, according to the context and the level of accuracy. The simplest and most common approach is based on force-based static assessment referred to in several regulations [8,10,70]; more advanced methods have been developed in the literature, e.g., direct displacement-based seismic design [51], and experimental assessment represents the most reliable method [63].

The safety verification parameters are expressed by considering efficient damage measures (DMs), engineering demand parameters (EDPs), and intensity measures (IMs), depending on the recommended or target level of verification and on engineering judgement. Regulations and codes define relevant IMs and associated thresholds as seismic demand measures for the relevant LSs. DMs and EDPs could be selected and estimated as a function of the relevant IM levels, for each LS. Capacity measures, often referred to fragility estimations [71,72], can be identified as IMs, EDPs, and DMs associated with the occurring of the relevant DS, associated with LSs; more often, EDPs and DMs are considered rather than IMs. The identification of the capacity measures strongly depends on the specific assessment methods, as it is discussed in the following paragraphs.

2.2. Damage measures, engineering demand parameters, and intensity measures

Verifying the seismic safety conditions using DMs, EDPs, or IMs corresponds to checking the safety conditions considering, as a reference, a different object of interest, i.e., NE, structure, and ground level, respectively. IMs capture the key characteristic(s) of the earthquake ground motions, EDPs are associated with structural response quantities that can be used to estimate damage to structural and nonstructural components, and DMs describe the physical and damage condition of NEs [73,74]. The seismic safety assessment of NEs is typically only described in terms of approach or general methodology in the codes, and the selection of the verification levels is not addressed.

For generic acceleration-sensitive NEs, the component-based level seems to be the most common one (using DM as a parameter). As a matter of fact, the basic assessment of NEs, i.e., implementing an equivalent static force verification [9], expresses the seismic demand as an inertial force applied on NE and considers the capacity as a measure that is directly associated with the NE response. For unanchored components, EDPs or IMs are often considered as capacity/demand measures if the elements are supported by structures or directly by the ground, respectively [37,39], but there are studies in which IMs are used to express the capacity of elements housed within buildings [38]. It should be noted that, assuming a reasonable reliability and robustness of the recommended methods for passing from DM to IM and vice versa means that the verification levels can be meant to be fully equivalent.

Several methods allow to correlate IMs, EDPs, and DMs, i.e., analytical, experimental, code formulation-based, observational, and mixed methods. In other words, given a ground-structural-nonstructural system, it is often possible to express the same condition through IMs, EDPs, and DMs thresholds by considering reasonable hypotheses and reliable methods. Analytical methods allow to assess the structural response (EDPs) as a function of the ground response (IMs) (structural analysis), and they can be extended to NEs to assess the NE response (DMs) as a function of the structural one (EDPs) (nonstructural analysis), following a cascading approach [39]. Extremely complex models could be developed to account for structural-nonstructural, ground-structural, ground-structural-nonstructural interactions. Therefore, analytical methods potentially interconnect IMs, EDPs, and DMs considering their significance in terms of both demand and capacity measures, where the interconnection can be relatively direct for demand and more indirect for capacity. In other words, the analysis can be meant as a transfer of the seismic demand from IM to EDP or DM, and the analysis level associated with the (conventional) achievement of the DSs identifies the (analytical) transfer from IM to EDP or DM in terms of seismic capacity. The identification of the DS occurrence through analytical methods can be carried out through (a) the implementation of experimental damage correlations, (b) a relatively accurate analytical capacity assessment (e.g., stress or strain analysis), or (c) reasonable conventional capacity thresholds, based on engineering judgment. Regarding methods (b) and (c), accurate analytical/numerical models and conventional thresholds should have had an early/original experimental validation.

Similarly to analytical methods, experimental methods potentially allow to assess the structural and nonstructural response and interconnect IM, EDP, and DM in terms of both seismic capacity and demand [36,75]. Differently from the analytical methods, experimental methods implement a more robust identification of DS occurrences, based on observation, inspections, and experimental data elaboration. However, in terms of feasibility, it is easier to interconnect EDPs to DMs (and vice versa), whereas it is more complicated to transfer IMs to EDPs (and vice versa). As a matter of fact, experimental tests on NEs often do not account for the structural response, e.g., NEs are tested as they were directly subjected to ground or floor motions [4,75]; in very few cases, the whole structural-nonstructural systems were tested [76], allowing to fully interconnect IMs, EDPs, and DMs.

Formulations developed in the literature or defined by regulations/

codes/documents often provide correlations among IM, EDP, DM, especially with regard to acceleration- and force-based parameters. The formulations are used as seismic demand assessment tools according to the typical purpose and methods of development. These formulations are often defined in regulations and codes [9,10,77] or were estimated in literature studies, considering various building scenarios [11,13,55,78,79]. These formulations are often expressed as a function of hazard, site, building, and nonstructural parameters, and they can be from relatively simple to complex. Seismic demand spectral response referred to within shake table protocols might also be used to interconnect IMs, EDPs, and DMs [63,80,81].

Observation and recorded data often provide correlations between seismic demand IMs and EDPs, e.g., ground and building acceleration peaks in instrumented buildings under real earthquakes [82], and observation and post-event surveys potentially correlate capacity measures of DM, EDP, and IM, e.g., by identifying parameter thresholds associated with the observed nonstructural damage exhibited in real buildings under earthquakes. Hybrid approaches can be defined by combining the abovementioned methods, e.g., by calibrating through experimental tests the dynamic properties of NEs to implement code-based seismic demand formulations (e.g., [61]).

2.3. Parameter selection and damage sensitivity of nonstructural elements

The definition of the relevant assessment parameters overall depends on the type and nature of structure and NEs, especially for EDP and DM measures. The literature provides several potential measures and parameters (e.g., [37,63,83,84]), and, generally, the relevant damage mechanisms and the related damage sensitivity of the NE represent an indication for the selection of efficient EDPs and DMs for performing seismic assessment. For example, the in-plane response/damage of infills and partitions is typically well correlated with interstory-drift ratio (IDR), as an EDP, whereas the out-of-plane response/damage is associated with floor acceleration, as an EDP, or component acceleration, as a DM [85,86]. However, it should be noted that interaction of the relevant damage mechanisms might condition the response of NE (e.g., this is also the case of infills [87]). Regarding IM, this is less associated with NEs and more associated with the structure, and this is typically defined by the regulations or codes, as previously mentioned.

2.4. Assessment procedure and uncertainty

In this subsection, EDP is considered as a measure for the seismic assessment check for sake of simplicity, even though the discussion can be equivalently extended to IM or DM. As previously mentioned, $EDP_{c,LS}$ defines the threshold value associated with the occurring of DS that is relevant to LS, which might be expressed by the earliest condition among multiple damage criteria. $EDP_{d,LS}$ represents the threshold value corresponding to the seismic demand relevant to LS, compatible with DS of interest. Generally, the determination of $EDP_{c,LS}$ can be carried out through multiple methods, i.e., experimental (reference method) [4,5], numerical/analytical [88,89], observational [90,91], mixed, and code-based [63,92] and generally strongly relies on engineering expertise and judgement. $EDP_{d,LS}$ should be estimated according to regulation or code prescriptions, relevant formulations developed in the literature (e.g., statistical models), or robust advanced methods for more accurate estimations or for critical scenarios, e.g., structural analysis or real records (e.g., ground or floor motions). Both $EDP_{c,LS}$ and $EDP_{d,LS}$ can directly or indirectly account for the uncertainty that conditions the capacity and the demand measures, respectively. In the former case (direct control), the uncertainty sources should be explicitly considered in the framework of the capacity or demand assessment, whereas, in the latter case (indirect control), code or literature prescriptions or indications should be referred to for correction factors or coefficients that implicitly implement a known or an unknown (reasonable) level of safety associated with the relevant sources of uncertainties. Modern codes provide very reduced or even null guidance for the assessment of the abovementioned measures and for controlling the uncertainties; therefore, the methodologies and regulatory recommendations associated with structural assessment, together with the engineering judgment and the experience have to be considered as a basic reference, at least regarding the general frameworks.

To directly account for the uncertainty, the uncertainty sources effects should be implemented in the capacity and demand assessment procedures as an input, conditioning the assessment process and determining the quantitative influence on the capacity and demand measures, given the uncertainty hypotheses. In this case, the input uncertainties should be carefully identified and consistently characterized in order to be reasonably representative of the potential significant capacity and demand scenarios. The selection of the sources of uncertainty to account for strongly depends on the specific applications and relies on both desired level of accuracy (and economic advantage) and engineering judgement. Obviously, in case relevant sources of uncertainties are not considered, the capacity and demand measure estimation should be conservative with regard to the not accounted uncertainty source. In the case of indirect uncertainty control measures, global or partial safety factor approaches could be implemented, referring to relevant regulation references, if available, or considering the methods defined for structural assessment, for lack of methods specific for NEs. The global approach is generally expressed by a global reduction factor/coefficient applied to $EDP_{c,LS}$ and/or by a global incrementation factor/coefficient applied to $EDP_{d,LS}$. The partial approach is based on the modification of the basic parameters or properties needed for the assessment of the capacity and the demand measures, which can correspond to reduction if the abovementioned parameters or properties positively affect $EDP_{c,LS}$ and incrementation in case of negative effect on $EDP_{d,LS}$. For structures, the use of partial safety factors is typically based on semi-probabilistic methods (e.g., [8]). Since current codes do not provide safety factors for NEs, advanced analytical or experimental methods could be implemented to estimate reasonable factors to be applied in the framework of simpler methods, e.g., force-based assessment, according to the relevant structural/nonstructural scenarios [52,58].

2.5. From the assessment framework to the technical implementation

The process of verification should be implemented considering LSs that are required to be verified by the relevant regulations/codes or, in the case of an advanced assessment, considering LSs of technical-scientific interest [78]. Generally, for newly designed ordinary buildings, DLS and LSLS should be verified among the serviceability and ultimate LSs, respectively, whereas OLS and NCLS should be typically considered for critical and existing buildings and facilities, respectively, in addition to the (basic) abovementioned LSs [52]. Even though serviceability LSs are typically more critical for NEs, ultimate LSs can also be relevant if the response or damage of NEs could potentially cause injuries and fatalities [52]. The abovementioned verification approach and requirements are provided by the relevant codes [8,9]. In particular, the Italian building code [10,77] generally requires two types of verifications: stability and functionality ones, and specifies facility importance and the elements that should be assessed. For ordinary buildings, NE should only be assessed considering the stability condition corresponding to life safety LS, whereas in case of strategic/critical buildings, plants/facilities and fixed elements (most NEs) should also be assessed with regard to the functionality conditions, corresponding to OLS [93].

The level of seismic demands associated with PLs and LSs is often meant to be conditioned by the importance/relevance of the facility or element to be assessed. Different approaches associating seismic demand levels to LSs are implemented in the regulations criteria. Some approaches, such as the one defined in the US codes [9,70], correlate the LS earthquake exceedance probability over a fixed lifetime to the performance level and account for the importance of the facility; this approach was probably introduced in early studies and reports (e.g.,

[94]). Other approaches, such as the Italian one, associate the earthquake exceedance probability over a lifetime, which increases as the importance of the facility grows (through an importance factor), but these do not vary the exceedance probability as a function of the importance of the facility or of the element. According to the Eurocode 8 [8], the seismic demand is amplified considering an element importance factor (not defined by the Italian building code but defined in ASCE 7) and the exceedance probability does not depend on the importance of the facility (as reported in the Italian building code) but the higher building importance is accounted for by amplifying the design reference peak ground acceleration.

In terms of LS to DS correlation for NEs, it is worth mentioning that serviceability LSs are typically relevant to NE responses that should be essentially elastic (e.g., OLS) or associated with incipient yielding (e.g., DLS), where yielding has a general significance and is meant as significant stiffness degradation. Ultimate LSs might be referred to the inelastic response since inelasticity of NEs was proven to reduce seismic demands, in terms of accelerations [44,45,47,54], and could be implemented as a seismic protection strategy, providing adequate strength, ductility, and dissipation conditions [45,47]; such an approach is currently present in the Eurocode 8 draft [48]. It is reasonable to assume that the abovementioned condition is consistent if both the following conditions are applicable: (a) NE is reasonably expected to retain inelastic capacities or sufficient ductility and (b) NE is expected to exhibit inelastic response for the relevant ultimate LSs without potentially causing major economic losses and/or human losses; as NE it is also meant the structural to nonstructural interface system, when applicable. Therefore, there might be cases in which NEs can be verified under ultimate LSs considering their elastic response, e.g., when at least one of the abovementioned conditions is not verified. In particular, the first condition (i.e. (a)) can be generally considered to be not applicable if (a1) there is no information regarding the inelastic capacities or (a2) the available information is compatible with reduced or negligible inelastic capacities. The second condition (i.e. (b)) is overall not applicable if one of the following condition is verified: (b1) NE is considered to be extremely critical or valuable and must not be even minorly damaged (e.g., museum objects and medical equipment), (b2) the inelastic behavior incursion is reasonably to be associated with life treats or, more generally, to major losses (e.g., heavy suspended equipment that might fall and cause casualties), and (b3) the facility in which NE is installed/located is extremely critical or has a strategic role and even minor functioning disruption must be prevented (e.g., hospital emergency departments).

Generally, elastic-based assessment can carried out by force- or acceleration-based EDPs, whereas displacement-, deformation-based EDPs, or derived measures (e.g., ductility) can be more consistently used to assess the inelastic-based conditions [95]. However, in the framework of advanced assessment procedures that account for inelastic response, e.g., when the seismic capacity/demand is estimated through nonlinear dynamic analyses, force-based or acceleration-based measures can also be used to assess ultimate LSs (e.g., [78]). In other words, under dynamic inputs, if the NE response accounts for the inelastic behavior (e.g., experimentally or numerically), the abovementioned measures might also be referred to, with due consideration.

Once the relevant LSs are identified, the associated DSs are selected according to available knowledge (e.g., code requirements, current practice, or literature studies), also according to engineering judgement procedures. The definition of the relevant DSs, to be associated with LSs, depends on the nature of the NE behavior that is relevant to the LS condition, e.g., DS can be associated with elastic or inelastic responses, as it was previously discussed. According to the identified DSs, efficient EDPs should be selected, and they can be strictly correlated to DSs. The following stages include the estimation of $EDP_{c,LS}$ and $EDP_{d,LS}$, and the abovementioned general comments describe the potential estimation approaches.

In the following sections, the defined assessment framework is applied as a technical methodology, considering two categories of acceleration-sensitive NEs, in order to evaluate the seismic safety over a wide range of potential scenarios. Different scenarios are meant to account for NE variability within the same case study NEs (e.g., different geometry and dynamic properties), building and site scenarios (ordinary and critical facilities and low to high seismicity sites), NE to building combination scenarios, and record to record variability. In particular, Section 3 describes the case study sites, buildings, and NEs, as well as it reports PLs and LSs of interest, as well as it reports seismic demands associated with the case study NEs and site/building scenarios. Section 4 reports the methodology and the results associated with the assessment of the seismic response and capacity of the case study NEs, i.e., RBs and SDOF systems. The association of PLs/LSs and damage states (DSs) is also defined in Section 4. The results of the safety assessment are presented and discussed in Section 5.

3. Case study scenarios and performance levels

3.1. Seismic hazard and building scenarios

High-, medium-, and low-seismicity sites in Italy were considered, referring to L'Aquila (AQ), Naples (NA), and Milan (MI) sites, respectively; soil type "C" and topography category "T_1", as defined in the Italian building code [10], were assumed: soil type "C" corresponds to an average velocity of the shear waves in the upper 30 m between 180 and 360 m/s, and topography category "T_1" is associated with a flat topography. Both ordinary and critical buildings were investigated; the former is typically associated with residential buildings, whereas the latter can be referred to hospital facilities or museum buildings. According to the Italian building code [10], the return period (T_R) used to estimate the seismic demands associated with the relevant LSs is computed considering a target earthquake probability of exceedance (P_{VR}) (fixed for each LS) over a reference period (V_R), equal to the product of the nominal life (V_N) and the importance coefficient (C_u). For ordinary (strategic/critical) buildings, V_N and C_u were assumed to be equal to 50 (100) years and 1.0 (2.0), resulting in V_R equal to 50 (200) years, respectively. Since V_N and C_u associated with strategic/critical are associated with the most severe condition, the abovementioned buildings are referred to as critical in the paper. P_{VR} associated with OLS, DLS, and LSLS (SLO, SLD, and SLV, in Italian [10]) is equal to 81 %, 63 %, and 10 %, respectively, resulting in T_R equal to 30, 50, and 475 (120, 201, and 1898) years, for ordinary (critical) buildings, respectively. The seismic design accelerations at bedrock (a_g) associated with the case study sites, building, and LSs are reported in Table 1.

3.2. Nonstructural elements

Acceleration-sensitive NEs are considered as a reference, and both unanchored or freestanding and anchored elements were considered to cover two macro categories of acceleration-sensitive NEs housed or installed within buildings. Unanchored NEs consist in relatively rigid elements and components that are simply supported by the building (floors), also referred to as freestanding elements. This category includes but is not limited to museum artifacts, laboratory and hospital equipment, unanchored mechatronic and hydraulic equipment, archive and office shelving/storage systems, architectural parts/decorations, and generic building contents and furniture. Anchored NEs are representative of NEs that are fixed or mechanically connected to the structures (also through secondary systems), such as base-anchored equipment, ceiling and lighting systems, projectors, antennas, billboards, plant installations, antennas, and other anchored systems.

Some assumptions were made for the technical identification of the case study models. In particular, unanchored NEs were meant to be modeled as relatively slender rigid blocks (RBs), assuming that their seismic response can be modeled by a pure rocking behavior. As a matter of fact, several freestanding NEs housed in buildings have relatively

Table 1
Seismic design acceleration at bedrock (a_g) corresponding to operativity limit state (OLS), damage limitation limit state (DLS), and life safety limit state (LSLS) conditions, according to the Italian building code [10].

Site	Longitude	Latitude	a_g					
			[g]					
			Ordinary buildings			Critical buildings		
			OLS (T_R = 30 years)	DLS (T_R = 50 years)	LSLS (T_R = 475 years)	OLS (T_R = 120 years)	DLS (T_R = 201 years)	LSLS (T_R = 1989 years)
L'Aquila	13.399	42.349	0.079	0.104	0.261	0.153	0.191	0.415
Naples	14.268	40.854	0.045	0.059	0.168	0.094	0.120	0.259
Milan	9.186	45.465	0.019	0.024	0.051	0.034	0.039	0.072

large slenderness [96], and in many cases, relatively large friction at their base [40]. This results in rocking-governed motion, which can often be robustly modeled as pure rocking behavior [89]. Several unanchored elements fall within this modeling assumption is terms of expected seismic behavior, mostly due to their stiffness and slenderness; some references supporting this modeling approach and applicability conditions can be found in [33,38,96]. Anchored NEs were modeled as SDOF systems, having an elastic-plastic response as described in the following sections. This assumption is more advanced and realistic than the typical assumptions made in the literature, also considering recent studies. As a matter of fact, acceleration-sensitive elements are often meant as linear elastic SDOF systems, and their safety is typically verified considering elastic response spectra and/or implementing deterministic assessment (e.g., [12,97]).

The characteristics of the case study NEs were derived from the literature and from past studies carried out by the authors. In particular, the reference for the RB and SDOF NEs can be found in [38,58–60]. A number of 10 RBs was considered, varying both semi-diagonal block size (R) and slenderness (h/b) over a representative range of scenarios. In particular, R, h/b and frequency parameter (p, defined in the following sections) range within 0.36–4.57 m, 1.96–7.82, and 1.27–4.52 Hz, respectively, where h and b are the base and height block dimensions, respectively; Table 2 reports the geometry parameters.

Case study SDOF systems consist in 12 cantilever models, fixed at their base and with an applied mass on their free end. The cantilevers were assumed to have S275 hollow square steel (HSS) sections (with dimension d and thickness t), with elastic frequency (f_a), height (H), and mass (m) ranging from 1–9 Hz, 1.0–4.5 m, and 0.04–0.35 t; the models were grouped into frequency ranges. Table 3 reports the structural details of the SDOF models. The models could be representative of a wide range of anchored NEs exhibiting a relatively ductile behavior, and further details can be found in D'Angela et al. [58].

3.3. Performance levels and limit states

Three PLs were considered: (1) operativity, (2) damage limitation, and (3) life safety. PL1 is associated with the full operativity of the facility following the seismic event, without the need for repositioning or repair intervention or with the need for very minor interventions, possibly implemented within few minutes. PL2 is associated with relatively significant repair/recalibration/replacement interventions, which can compromise the functioning of the facility, to be possibly implemented within few to several days; however, PL2 is not potentially associated with major economic losses and life safety treats. Finally, PL3 is related to severe damage of NEs and, in case it is exceeded, it implies major economic losses and possible injuries/fatalities. Accordingly, PL1 and PL2 are associated with serviceability LSs, OLS and DLS, whereas PL3 is associated with ultimate LSs, i.e., LSLS. The collapse condition was not explicitly investigated since this is less significant for NEs. PLs were correlated to DSs that were relevant to the seismic response and damage of the case study NEs. The quantitative specification of the DSs is described in the methodology sections of the seismic response and capacity section (Section 4), i.e., Sections 4.1.1 and 4.2.1 corresponding to RBs and SDOF systems, respectively. It should be noted that PLs and DSs were defined only considering the structural and dynamic response of the elements, without accounting for electric/electronic operativity or functioning other than structural response and integrity levels. As a matter of fact, the latter DSs should be associated with specific elements to assess and should be provided by the producer, according to experimental tests or reliable advanced analytical methods. However, the methodology and the results are generally applicable, and they could be applied with regard to specific damage criteria.

Table 3
Case study single-degree-of-freedom (SDOF) systems: geometric and structural details [58].

Model ID	Range [−]	f_a [Hz]	d [mm]	t [mm]	H [m]	m [t]
SDOF-1A	I	1.02	70	3.0	4.50	0.10
SDOF-1B		1.03	60	3.0	2.50	0.35
SDOF-1C		1.13	50	2.5	3.00	0.08
SDOF-2A	II	1.48	70	3.0	3.50	0.10
SDOF-2B		1.52	60	3.0	2.50	0.16
SDOF-2C		1.52	60	2.5	3.00	0.08
SDOF-3A	III	2.97	70	3.0	2.20	0.10
SDOF-3B		3.04	60	3.0	2.50	0.04
SDOF-3C		3.06	90	3.0	3.00	0.08
SDOF-4A	IV	5.86	70	3.0	1.40	0.10
SDOF-4B		7.34	80	4.0	1.50	0.10
SDOF-4C		9.02	70	3.0	1.05	0.10

3.4. Seismic demand

The seismic demand associated with RBs and SDOF systems was assessed according to the Italian building code [10]. Both PGA and PGV were considered as demand IMs, as well as PFA was also accounted for as a demand EDP. For RBs, PGA, PGV, and PFA were expressed as dimensionless measures, as it is described in Section 4.1.1. Demand PGV was estimated according to Eq. (1), which was defined in the Italian building code [10], where S is the stratigraphic coefficient, and T_C is the

Table 2
Case study RBs: geometry parameters [38,59,60].

Model ID		RB-1A	RB-1B	RB-1C	RB-1D	RB-1E	RB-2A	RB-2B	RB-2C	RB-2D	RB-2E
R	[m]	0.36	0.72	0.72	0.72	1.43	1.52	3.05	3.05	3.05	4.57
h/b	[−]	3.92	1.96	3.92	7.83	3.92	5.00	2.50	5.00	7.50	5.00
p	[Hz]	4.52	3.20	3.20	3.20	2.27	2.20	1.55	1.55	1.55	1.27

spectral period as defined in the code.

$$PGV = 0.16 \cdot a_g \cdot S \cdot T_C \quad (1)$$

PFA was assessed according to the simplified formulation (SF) of the seismic demand provided by the Italian building code [77], developed in literature studies [13], not reported for the sake of brevity. Assuming the NE installed at the roof of the building (i.e., the most severe condition) PFA to PGA ratio is assumed to be equal to two. It should be noted that this latter ratio could be higher than two in some cases, especially under linear elastic building response [9,68,98]; however, the (lognormal model) median PFA to PGA ratio associated with records considered for RBs and SDOF systems was equal to 2.30 and 2.18, respectively, confirming the compatibility with the PFA to PGA ratio assumed according to the Italian building code.

Fig. 1 depicts the seismic demand in terms of PGA, PGV, and PFA for the considered LSs and site/building scenarios, as a function of T_R; it is recalled that T_R corresponding to OLS, DLS, and LSLS is equal to 30, 50, and 475 years for ordinary buildings, and to 120, 201, and 1898 years for critical buildings, respectively.

In case safety assessment is preferred to be performed considering peak component acceleration (PCA), seismic demand can be referred to (pseudo-)spectral acceleration (Sa), estimated according to relevant codes. Code formulations of seismic demands (Sa) are typically expressed as a function of fundamental building period (T_1), which might not be known or might not be of interest for general or not specific design/assessment or qualification procedures. In these latter cases, it is possible to conservatively apply an envelope of SF, developed in [62] as a required response spectrum (RRS) for NE seismic assessment and qualification purposes. Eq. (2) reports the envelope formulation, where α_g is the LS design PGA on stiff soil expressed in g unit, z is the NE installation height within the building, H_B is the building height, f_{NE} is the NE (fundamental) elastic frequency, and f_0, f_1, and f_2 are frequency constants, equal to 1.00, 1.40, and 12.5 Hz, respectively.

$$\frac{Sa}{(\alpha_g S)} = \begin{cases} 4\,(1+z/H_B) + \dfrac{(1+z/H_B)}{(f_1 - f_0)}\,(f_{NE} - f_0) & \text{for } f_{NE} < f_1 \\ 5\,(1+z/H_B) & \text{for } f_1 \le f_{NE} < f_2 \\ \left[\dfrac{5\,(1+z/H_B)}{1+4\left(1-\frac{f_2}{f_{NE}}\right)^2}\right] & \text{for } f_{NE} \ge f_2 \end{cases} \quad (2)$$

For a more general expression, which also accounts for NE fundamental frequency (f_{NE}) lower than 1 Hz (not considered in Zito et al. [62]), f_0 could be conservatively set equal to 0.75 Hz instead of 1.00 Hz (valid for f_{NE} not smaller than 0.75 Hz).

4. Seismic response and capacity of case study nonstructural elements

4.1. Rigid blocks

4.1.1. Methodology

The seismic capacity of RBs was assessed by processing the results of an extended numerical analysis campaign carried out by the authors [38,59] and implementing a novel methodology, defined in the following. RBs were modeled through the motion equations developed by Housner [24], implemented in the literature since early times [17,26,99] and, nowadays, still widely used [89,100,101]. The motion equation is reported in Eq. (3), where θ is the block rotation angle, p is the frequency parameter (Eq. (4)), α is the critical angle (Eq. (5)), $\ddot{u}_g(t)$ is the time history base acceleration input, and g is the gravity acceleration constant. R and p were considered as key dynamic parameters (DPs) of the investigated RBs.

$$\ddot{\theta}(t) = -p^2 \left\{ \sin\left[\alpha\ \mathrm{sgn}(\theta(t)) - \theta(t)\right] + \frac{\ddot{u}_g(t)}{g} \cos\left[\alpha\ \mathrm{sgn}(\theta(t)) - \theta(t)\right] \right\} \quad (3)$$

$$p = \sqrt{\frac{3\,g}{4\,R}} \quad (4)$$

$$\alpha = \tan^{-1}\left(\frac{b}{h}\right) \quad (5)$$

An unitary coefficient of restitution is considered, where this latter is defined as ratio of the kinetic energy prior to and after the impact; this is generally a conservative assumption [40]. The motion equation was numerically solved through the Runge–Kutta ordinary differential equation (ODE) solver in MATLAB [102]. Incremental dynamic analyses were carried out up to the failure, considering both real ground and floor motions as loading histories; peak acceleration was considered as an analysis IM, and dimensionless peak block rotation ($|\theta_{max}/\alpha|$) was used as a damage measure (DM). Generally, $|\theta_{max}/\alpha|$ is meant to be an EDP, but in this context, EDPs are measures of demands on NEs (transferred through the building) that are associated with the structural response due to IMs (ground measures). The seismic response of the case study RBs subjected to ground and floor motions (both real and shake table protocol-based) was assessed in terms of IDA curves [60] and fragility parameters [38], also taking into account the influence of the building response.

Real ground and floor motions were considered as loading histories, and these were derived from past studies. A set of strong ground motions (SGM set) was considered, including strong real records provided by the ATC 63 database [103–105], associated with magnitude larger than 6.5, PGA larger than 0.2 g, and PGV larger than 15 cm/s. SGM set includes 44 far field (FF) and 28 near field (NF) records (with and without pulse); details regarding SGM set can be found in [40,59], and related set

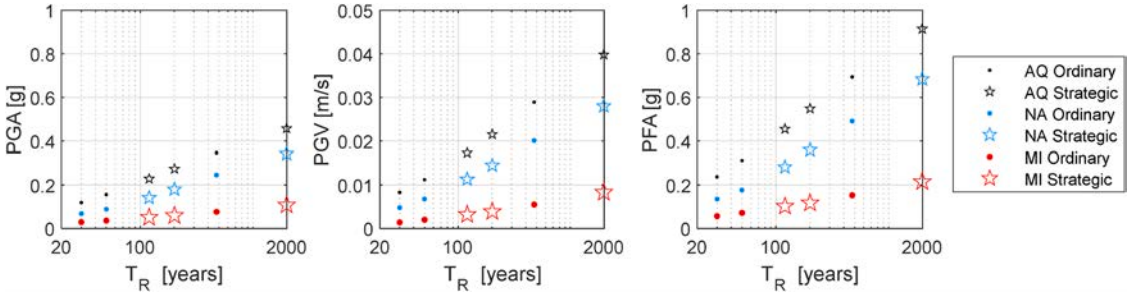

Fig. 1. Seismic demand, expressed in terms of peak ground acceleration (PGA), peak ground velocity (PGV), and peak floor acceleration (PFA), associated with operativity limit state (OLS), damage limitation limit state (DLS), and life safety limit state (LSLS), as a function of return period (T_R), considering L'Aquila (AQ), Naples (NA), and Milan (MI) sites and ordinary and critical buildings.

spectral accelerations (Sa) are depicted in Fig. 2 as a function of frequency (f).

Two sets of floor motions were considered: mild-to-strong floor motions (FM set) and strong floor motions (SFM set). FM set includes real inputs recorded in instrumented buildings, provided by the CESMD database [82]. The selected records refer to US reinforced concrete (RC) buildings (built in 1923–1975), and they are associated with PFA larger than or equal to 0.05 g and with the most amplified response within the building (roof level for all signals but one). FM set includes 12 FF and 12 NF records, equally accounting for low-, medium-, and high-rise building cases. FM set includes seven signals related to PGA larger than or equal to 0.2 g, which defines the SFM set, in order to considering a more severe response, relatively more comparable with SGM set. Further details regarding FM and SFM sets can be found in [38,60]; Fig. 2 shows Sa vs. f for FM sets.

Capacity curves and surfaces were defined in this study in terms of fitted statistical-based capacity IM measures (component fragilities) as a function of incremental DSs and (multiple) RB parameters. In particular, dimensionless peak ground acceleration (PGA* in Eq. (6)) and dimensionless peak ground velocity (PGV* in Eq. (7)) were considered as IMs. PGV* was also considered as IM since it was found to be well correlated with RB dynamics, especially for medium to large size blocks (e.g., [38,40]).

$$PGA^{*} = \frac{PGA}{g\ \tan(\alpha)} \tag{6}$$

$$PGV^{*} = \frac{p\ PGV}{g\ \tan(\alpha)} \tag{7}$$

The fragility curves, used to estimate the abovementioned capacity curves, were computed by assuming a lognormal model, according to Porter [72]. The median curves, expressed in terms of PGA* and PGV*, were associated with several DSs, and achievement of DS was identified according to Eq. (8), where DM_{dyn} represents relevant peak dynamic response and DM_{lim} related capacity. In particular, DM_{dyn} corresponds to $|\theta_{max}/\alpha|$ associated with the dynamic analyses and DM_{lim} is $|\theta_{max}/\alpha|_{lim}$, i.e., the capacity limit threshold; a number of 12 DSs was considered to investigate in detail the whole rocking amplitude spectrum, from incipient rocking to overturning, passing through intermediate rocking amplitudes, i.e., $|\theta_{max}/\alpha\ |_{lim}$ equal to 0.01, 0.05, 0.1 to 1.0 through 0.1 increments.

$$DM_{dyn} \geq DM_{lim} \tag{8}$$

$|\theta_{max}/\alpha|_{lim}$ was set equal to 0.1, 0.2, 0.4, and 0.8 corresponding to DS1, DS2, DS3, and DS4, respectively, by critically synthesizing the relevant literature (e.g., [37,39,59]). In particular, DS1, DS2, DS3, and DS4 are associated with absent or negligible damage, minor damage, moderate damage, and severe damage, respectively. As a matter of fact, θ_{max}/α exceeding 0.10 was correlated to limited rocking in [37], 0.2 to 0.4 range refers to moderate rocking and potential moderate to severe damage [59,106], and a value exceeding 0.8 is likely to be associated with highly unstable behavior and severe damage [38]. It should be noted that $|\theta_{max}/\alpha|_{lim}$ larger than the threshold associated with DS4 (i.e., 0.8) is not associated with PLs and LSs since collapse conditions were not investigated, as previously mentioned (Section 3.3). However, the abovementioned damage conditions were investigated for scientific reasons, and the complete overturning of the blocks (i.e., $|\theta_{max}/\alpha|_{lim}$) equal to one is referred to DS5.

The capacity curves were expressed as fragility parameters (FPs), i.e., fitted fragility median (x_M) and logarithmic standard deviation (σ) values as a function of block geometry or frequency-based parameters, for both PGA* and PGV*, for all investigated $|\theta_{max}/\alpha|_{lim}$ values and considering both ground and floor motions (SGM, FM, and SFM sets). The coefficient of determination (COD) was assessed to prove the quality of the fitting, and, in many cases, this resulted in high values. Capacity surfaces were assessed by expressing x_M, in terms of PGA* or PGV*, as a function of block geometry or frequency-based parameters and $|\theta_{max}/\alpha|_{lim}$, accounting for SGM, FM, and SFM sets. The use of PGA* and PGV* accounted for the influence of the building response, as discussed in the previous sections. As geometrical parameters, both R and α were assessed, as both p and free rocking frequency (f_r) were used as frequency-based measures; f_r was evaluated considering the classical theory expression of the rocking period T_r [24], assuming θ_0/α equal to 0.25 and 0.75 [59]. R and p resulted in higher efficiency in terms of correlation quality, compared to α and f_r, respectively; therefore, the elaborations were carried out considering R and p.

4.1.2. Results

Fig. 3 depicts x_M, in terms of PGA* and PGV*, expressed as a function of $|\theta_{max}/\alpha|_{lim}$ for SGM, FM, and SFM sets. The capacities are discussed in the following considering their significance and implications in terms of influence of (a) different nature of floor motions (i.e., SFM set and FM set) and (b) building amplification/filtering effect, even though the abovementioned figures represent quantitative measures of capacity themselves.

The PGA* capacities associated with SFM set are overall lower than

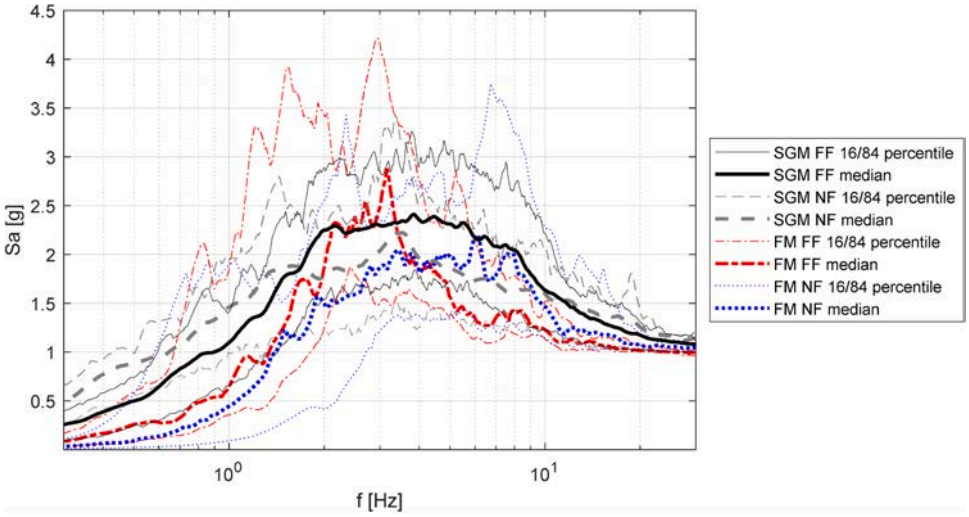

Fig. 2. Spectral accelerations *Sa* vs. *f* related to far field (FF) and near field (NF) records associated with strong ground motion (SGM) and floor motion (FM) sets, normalized considering peak accelerations equal to 1.0 g, considered for rigid block (RB) analysis [38].

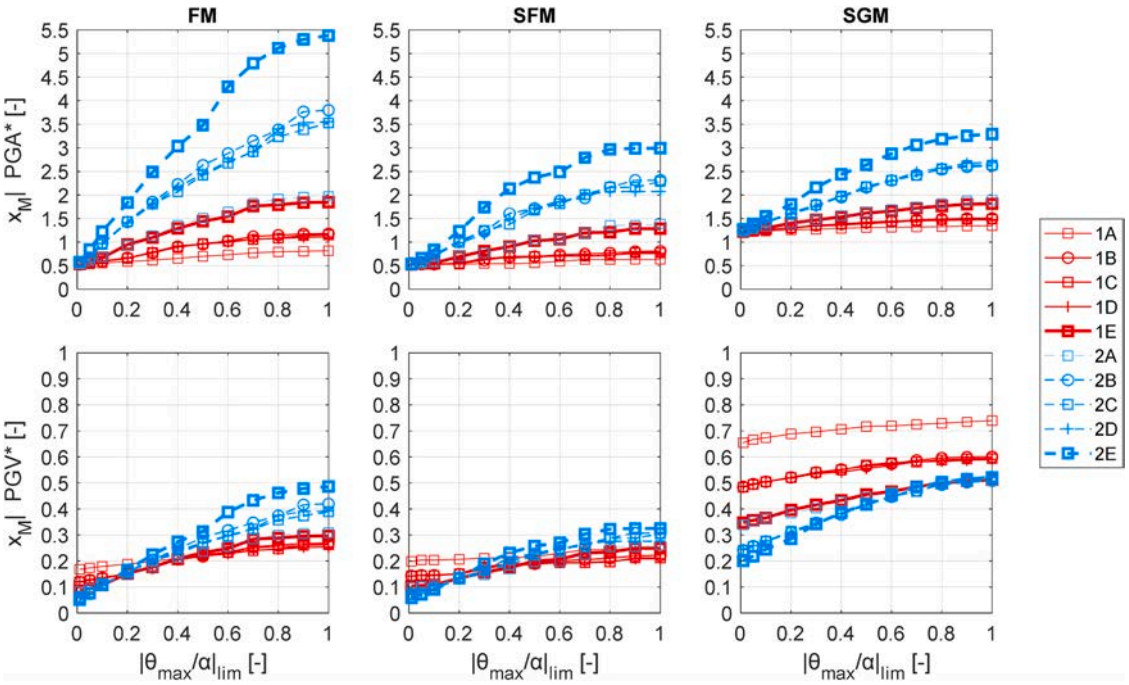

Fig. 3. Fragility median (x_M) in terms of dimensionless peak ground acceleration (PGA*) and dimensionless peak ground velocity (PGV*) associated with rigid blocks (RBs), as a function of limit dimensionless rocking amplitude angle ($|\theta_{max}/\alpha|_{lim}$) considering strong ground motion (SGM), floor motion (FM), and strong floor motion (SFM) sets.

the ones associated with FM set, as it was generally expectable, and the influence on the capacity significantly depends on both R and $|\theta_{max}/\alpha|_{lim}$. A (lower) higher relative severity of SFM, in terms of PGA* capacity reduction, is associated with the (smaller) larger blocks and (lower) higher $|\theta_{max}/\alpha|_{lim}$. In particular, for the overturning ($|\theta_{max}/\alpha|_{lim} = 1$) of the (smallest) largest block, i.e., (1A) 2E, the FM to SFM reduction factor in terms of PGA* capacity ($1 - \frac{SFM\ PGA*}{FM\ PGA*}$) is approximately equal to (23 %) 44 %, whereas, the reduction factor is null for rocking onset ($|\theta_{max}/\alpha|_{lim} = 0.01$); between rocking onset and overturning, the reduction overall gradually increases as $|\theta_{max}/\alpha|_{lim}$ grows, and the difference between the capacity reduction related to the smallest and largest block is relatively equal to about 20–25 % for $|\theta_{max}/\alpha|_{lim}$ larger than or equal to 0.05, whereas for a value equal to 0.01, the abovementioned difference is lower than 5 %.

The trend of the capacity reduction factor associated with PGV* ($1 - \frac{SFM\ PGV*}{FM\ PGV*}$) is qualitatively identical to the one associated with PGA*, as it is expected according to the implemented methodology, even though the quantitative significance related to PGV* is different from the case of PGA*, as it is discussed in the following. Considering PGV*, SFM are often but not always more severe than FM; in particular, corresponding to lower $|\theta_{max}/\alpha|_{lim}$, FM PGV* capacities are lower than SFM, especially for larger blocks; in particular, for all blocks and incipient rocking, SFM PGV* are 12–20 % larger than FM, whereas, for larger $|\theta_{max}/\alpha|_{lim}$ values, SFM to FM PGV* margin tends to decrease as $|\theta_{max}/\alpha|_{lim}$ increases, and the margin becomes negative (i.e., higher SFM severity) below a $|\theta_{max}/\alpha|_{lim}$ threshold, which increases as R decreases. For set 2 blocks (medium to large blocks), over $|\theta_{max}/\alpha|_{lim}$ larger than 0.05–0.1, SFM set is more severe than FM, in terms of PGV* capacity, and the highest reduction factor in capacity corresponds to overturning (and largest block), i.e., equal to 33 %. For set 1 block (small to medium block), SFM set is more severe than FM set for significantly larger $|\theta_{max}/\alpha|_{lim}$ values, which depend more significantly on R; for example, for block 1E (medium size block), the $|\theta_{max}/\alpha|_{lim}$ threshold is equal to 0.1 (comparable with set 2 blocks), whereas for block 1A (smallest block), the $|\theta_{max}/\alpha|_{lim}$ threshold is equal to 0.3; for blocks 1B, 1C, and 1D (having same R), the $|\theta_{max}/\alpha|_{lim}$ threshold ranges in 0.2–0.3. The minimum PGV* capacity reduction due to SFM corresponding to overturning is associated, as expected according to the previous comments, to the smallest block, and it is equal to about 7 %.

It is interesting to quantify the influence of the building amplification/filtering effect [38]. This can be assessed by comparing SFM and SGM capacities. Once again, it should be specified that the qualitative trend of the capacity reduction factor due to the influence of the building associated with PGA* ($1 - \frac{SFM\ PGA*}{SGM\ PGA*}$) and PGV* ($1 - \frac{SFM\ PGV*}{SGM\ PGV*}$) is similar, but the quantitative significance is different, as described in the following. Overall, PGA* (PGV*) capacity reduction factors decrease as $|\theta_{max}/\alpha|_{lim}$ grows with a magnitude that depends on R, and the factor value corresponding to incipient rocking does not depend on R: PGA* (PGV*) reduction factor is equal to about 55–58 % (70 %). Considering PGA* (PGV*), for smaller blocks (e.g., set 1 blocks but 1E), the reduction factor related to the overturning is slightly smaller than the one related to the incipient rocking, whereas, for larger blocks (set 2 blocks but 2A), the reduction factor associated with the overturning is significantly smaller than the incipient rocking one, i.e., equal to 10–33 % (38–40 %). In particular, the decrease in reduction factor due to the increase of $|\theta_{max}/\alpha|_{lim}$ is more gradual (e.g., linear) for set 1 blocks, whereas it is approximately bilinear for set 2 blocks, with a larger slope over small to medium $|\theta_{max}/\alpha|_{lim}$ values (e.g., $|\theta_{max}/\alpha|_{lim}$ smaller than or equal to 0.4–0.5).

Fig. 4 shows σ associated with PGA* and PGV*, as a function of $|\theta_{max}/\alpha|_{lim}$, considering FM, SFM and SGM sets. The trend and the values of σ significantly depend on the input set and on IM, as it was expected. Overall, σ related to FM is significantly higher than the one associated with the other input sets, for both PGA* and PGV*.

Regarding σ related to FM, the lowest values of σ (as a function of $|\theta_{max}/\alpha|_{lim}$) correspond to incipient rocking, whereas the highest is associated with overturning, as it was discussed in past studies. Considering PGA*, σ increases as $|\theta_{max}/\alpha|_{lim}$ grows, with a trend that is less gradual as R increases; in particular, for smaller R blocks, σ tends to gradually increase as $|\theta_{max}/\alpha|_{lim}$ increases (approximately linearly), whereas, for larger R blocks, σ tends to grow with $|\theta_{max}/\alpha|_{lim}$ according to a roughly bilinear trend, with a larger (smaller) slope associated with

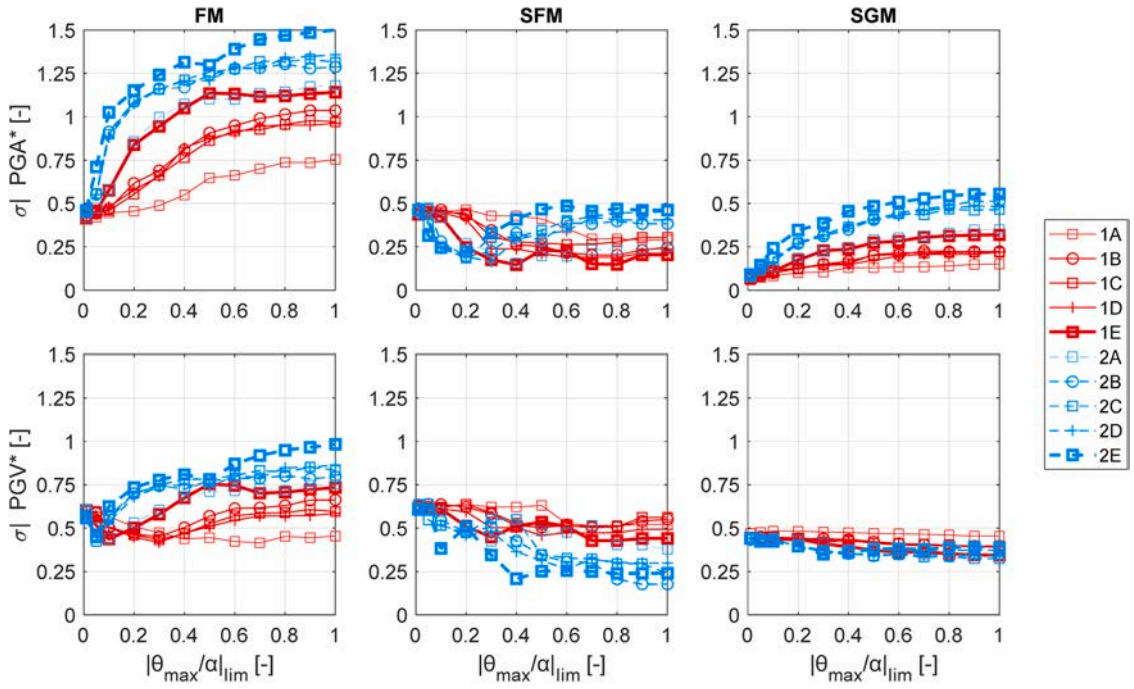

Fig. 4. Fragility logarithmic standard deviation (σ) in terms of dimensionless peak ground acceleration (PGA*) and dimensionless peak ground velocity (PGV*) associated with rigid blocks (RBs), as a function of limit dimensionless rocking amplitude angle ($|\theta_{max}/\alpha|_{lim}$) considering strong ground motion (SGM), floor motion (FM), and strong floor motion (SFM) sets.

lower (larger) $|\theta_{max}/\alpha|_{lim}$. PGA* σ values evolve from about 0.41–0.46 (incipient rocking) to significantly large values (overturning), which range within 0.75 (the smallest block, 1A) to 1.5 (the largest block, 2E). The σ trend associated with PGV* is significantly more irregular than the one related to PGA*, and the σ vs. $|\theta_{max}/\alpha|_{lim}$ are overall non monotonic. All blocks present a relative minimum point corresponding to a $|\theta_{max}/\alpha|_{lim}$ threshold that increases as R decreases: relative minimum $|\theta_{max}/\alpha|_{lim}$ is equal to (a) 0.05 for all set 2 blocks but 2A, (b) 0.1 for blocks 2A and 1E, (c) 0.3 for all set 1 blocks but 1A, and (d) 0.7 for block 1A; it is interesting to notice that the width of the relative minimum range (expressed in terms of $|\theta_{max}/\alpha|_{lim}$ range) increases as R decreases, and while for set 2 blocks but 2A is very narrow, this is extremely large for block 1A; the relative minimum is more associated with a plateau response. It is very interesting to notice that the σ value associated with the relative minima points is approximately the same for all blocks, e.g., equal to about 0.4, and this latter value is quite similar to the minimum σ value associated with PGA* (corresponding to incipient rocking). This highlights that the minimum uncertainty associated with PGV*, which depends on damage severity ($|\theta_{max}/\alpha|_{lim}$) as previously discussed, does not fall below the minimum uncertainty associated with PGA*, which always corresponds to incipient rocking. Several comments can be made regarding the different efficiency of PGA* and PGV*, expressed in terms of lower σ values, for the investigated dimensionless rocking amplitude angles ($|\theta_{max}/\alpha|_{lim}$). As it was already discovered in D'Angela et al. [38], the efficiency of the IMs strongly depends on the considered IMs and does not only depend on R, as it was found regarding the response subjected to ground motions [37,40]. PGA* is more efficient for incipient rocking (for all R values), and, in all other cases, PGV* is more efficient than PGA*, except for $|\theta_{max}/\alpha|_{lim}$ equal to 0.05 for set 1 blocks.

Despite SFM set also accounts for the ground record-to-record and building influence uncertainty sources, σ values associated with PGA* (more significantly) and PGV* (less significantly) are significantly lower than the ones related to FM set (Fig. 4); moreover, their trend is more complex than the ones related to FM set, especially considering PGA*. In particular, for all blocks and over the whole $|\theta_{max}/\alpha|_{lim}$ spectrum, σ related to PGA* is lower than 0.5 and is not larger than about 0.3 in several cases, i.e., set 1 blocks but 1A for $|\theta_{max}/\alpha|_{lim}$ larger than 0.2–0.3, block 1A for $|\theta_{max}/\alpha|_{lim}$ larger than 0.6, and set 2 blocks with $|\theta_{max}/\alpha|_{lim}$ between 0.1 and 0.3. In all cases σ vs $|\theta_{max}/\alpha|_{lim}$ is non monotonic, and this is more significant for set 2 blocks and less for set 1 ones, and for block 1A the response is substantially monotonic; clear relative minima points are identified for set 2 blocks and block 1E, with the related $|\theta_{max}/\alpha|_{lim}$ values in 0.2–0.4, whereas, for set 1 blocks but 1E, the trend is overall decreasing in $|\theta_{max}/\alpha|_{lim}$ without clear relative minima points. While for incipient rocking there is null σ dispersion associated with the different block sizes, considering larger rocking amplitudes, R has a major influence on σ (larger dispersion). The trend of σ associated with PGV* related to SFM is qualitatively similar to the response exhibited considering PGA*, even though some quantitative differences can be identified. Corresponding to incipient rocking, σ is essentially constant for the different R values, with a value just higher than 0.6. For larger $|\theta_{max}/\alpha|_{lim}$ values, σ related to set 2 blocks tends to decrease as $|\theta_{max}/\alpha|_{lim}$ grows, reaching relatively reduced values at the overturning, i.e., between 0.2 and 0.3 for all blocks but 2A. For set 1 blocks, σ decreases with less significance as $|\theta_{max}/\alpha|_{lim}$ grows, especially for smaller blocks, exhibiting a non-monotonic response for block 1E. Overall, overturning σ values related to set 1 blocks ranges between 0.4 and 0.6, with a value that increases as the R decreases.

The σ trend related to SGM (Fig. 4) does not represent a novelty regarding incipient rocking and overturning [40]. In particular, considering PGA*, σ related to small values of $|\theta_{max}/\alpha|_{lim}$ is significantly small (lower than 0.1) and does not significantly depend on R; for larger $|\theta_{max}/\alpha|_{lim}$, all blocks present σ regularly increasing as $|\theta_{max}/\alpha|_{lim}$, grows, increasing the block-related dispersion too; the increase with $|\theta_{max}/\alpha|_{lim}$ related to smaller blocks (set 1 blocks but 1E) is less significant, whereas, as R increases, σ increases more significantly; for larger blocks (set 2 blocks but 2A), overturning σ is between 0.5 and 0.6, whereas for smaller blocks (set 1 blocks but 1E), σ is between 0.15 and 0.25; the medium size blocks (1E and 2A) are associated with overturning σ equal to about 0.3. σ associated with PGV* is gradually decreasing as $|\theta_{max}/\alpha|_{lim}$ increases. σ related to PGA* is overall significantly lower than σ associated with PGV* over small values of

$|\theta_{max}/\alpha|_{lim}$. For larger blocks, as $|\theta_{max}/\alpha|_{lim}$ increases, PGV* σ tends to become smaller than the related PGA* value, and the $|\theta_{max}/\alpha|_{lim}$ threshold associated with the inversion of the efficiency trend increases as R decreases: threshold $|\theta_{max}/\alpha|_{lim}$ is equal to about 0.3 for 2E block and 0.4 for other set 2 blocks but 2A. For all other blocks, σ related to PGA* is always lower than PGV* one, even for overturning (where there is the maximum decrease in PGV* σ values). x_M and σ values depicted in Figs. 3 and 4, respectively, associated with PGA* and PGV*, were fitted considering both R and p, in order to define closed-form correlations. The fitted curves associated with x_M are referred to as capacity curves since they express the capacity of the NEs as a function of their geometrical/dynamic properties. A very efficient fitting was identified by three-degree polynomial correlations for all investigated cases, with COD values larger than 0.9 in most cases. The same curves were developed considering σ, but the curves are not depicted for the sake of brevity. The general expression of FP is reported in Eq. (9), where FP corresponds to x_M or σ, IM to PGA*, and PGV*, and DP to R or p. Fitting constants and related COD are reported in the Appendix.

$$FP|IM = C_{11}DP^3 + C_{12}DP^2 + C_{13}DP + C_{14} \quad (9)$$

Figs. 5 and 6 show the capacity curves considering PGA* and PGV* as an IM, respectively, as a function of R and p, considering SGM, FM, and SFM sets. Given the quantitative significance of the capacity curves, they are only briefly discussed in the following, identifying the quantitative relations among the investigated parameters, with particular focus on the influence of the input sets. Furthermore, the main tendencies were discussed referring to Figs. 3 and 4 with regard to the empirical data (markers in Figs. 5 and 6), and given the high quality of the fitting, the comments related to the fitting curves confirm and strengthen the abovementioned tendencies, especially with regard to R, which was explicitly discussed in the previous paragraphs.

The tendency of the PGA* capacity curves (Fig. 5) is more linear-like considering R, especially for SGM and SFM, whereas the third-degree polynomial tendencies of the curves related to p is more significant. For lower $|\theta_{max}/\alpha|_{lim}$ values, the capacity curves are overall constant over R and p, whereas, as $|\theta_{max}/\alpha|_{lim}$ grows, they tend to (decrease) increase with (p) R, with a magnitude that increases as $|\theta_{max}/\alpha|_{lim}$ grows. Among the possible remarks, it is noted that SGM curves are overall clearly higher than SFM ones for all spectrum of R and p, and difference between the abovementioned curves tends to decrease as $|\theta_{max}/\alpha|_{lim}$ increases, especially for low p and high R. It is interesting to highlight that FM curves tend to become higher than SGM ones as (p) R (decreases) increases, with a magnitude that grows as $|\theta_{max}/\alpha|_{lim}$ increases. In Fig. 5, it is clearly possible to identify threshold (p) R values that are associated with the inversion of the relative severity of FM curves, as compared with SGM ones, and quantitative comments are omitted for the sake of brevity.

Considering PGV* as an IM (Fig. 6), it can be noted that different relative trends are found with regard to the input sets. Firstly, it can be noted that SFM capacities are always significantly lower than SGM ones, differently for the case of PGA*, where for large R (small p), the difference is relatively small. Secondly, FM capacities are never higher than SGM ones, and, except for large R (small p), the difference between the abovementioned capacities is relatively large. In other words, FM capacity curves tend to increase more than other curves over large R (small p) values, but this increase is not sufficient for exceeding SGM capacities. Thirdly, as $|\theta_{max}/\alpha|_{lim}$ increases, the capacity curves tend to vary their trend as a function of R and p, especially for FM and SFM curves. In particular, the abovementioned curves have an overall global decreasing trend as R increases and a global increasing trend as p increases. As $|\theta_{max}/\alpha|_{lim}$ grows, the abovementioned trends are inverted, and the capacity curves globally increase as R increases and globally decrease as p increases, even though the behavior is actually nonmonotonic.

In order to account for the combination of $|\theta_{max}/\alpha|_{lim}$ and R (or p),

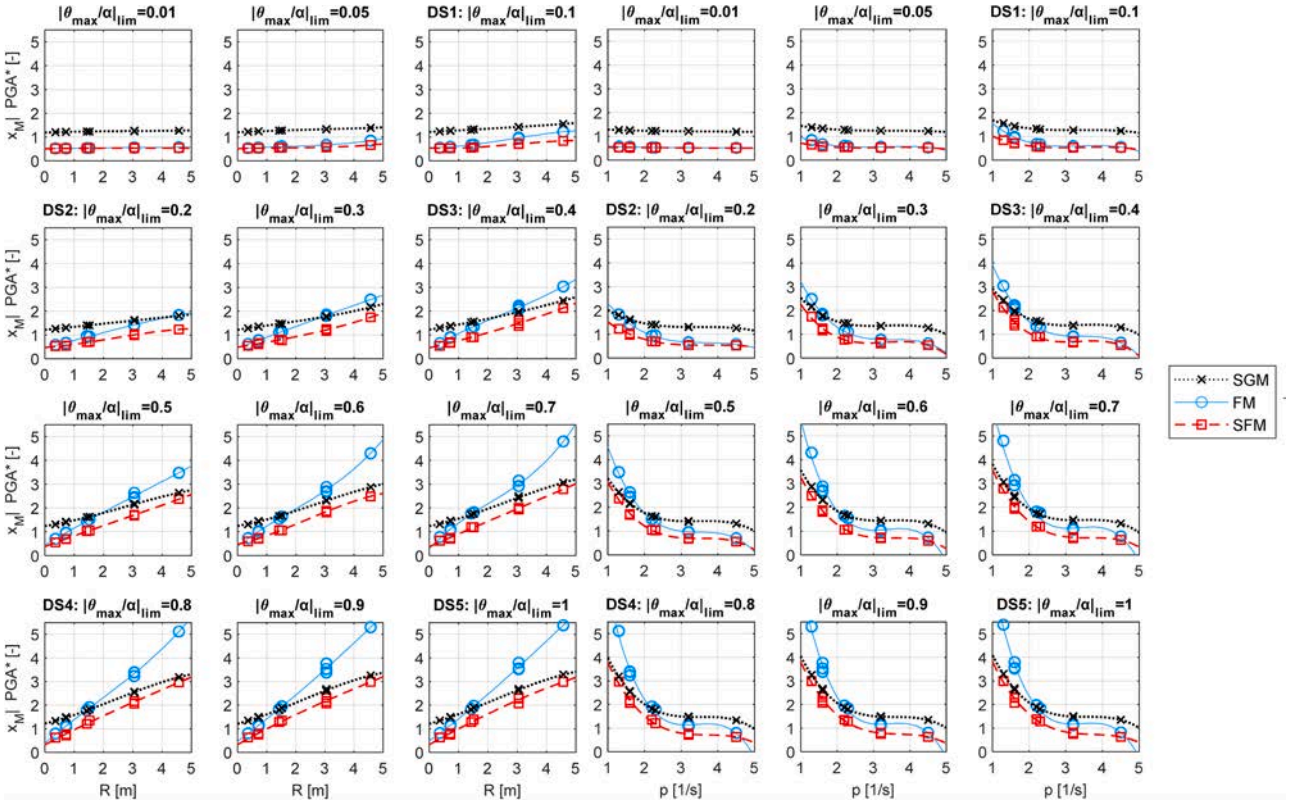

Fig. 5. Capacity curves (fragility medians (x_M)), expressed in terms of dimensionless peak ground acceleration (PGA*) associated with rigid blocks (RBs), as a function of semi-diagonal block dimension (R) or frequency parameter (p), for the investigated DSs, considering strong ground motion (SGM), floor motion (FM), and strong floor motion (SFM) sets.

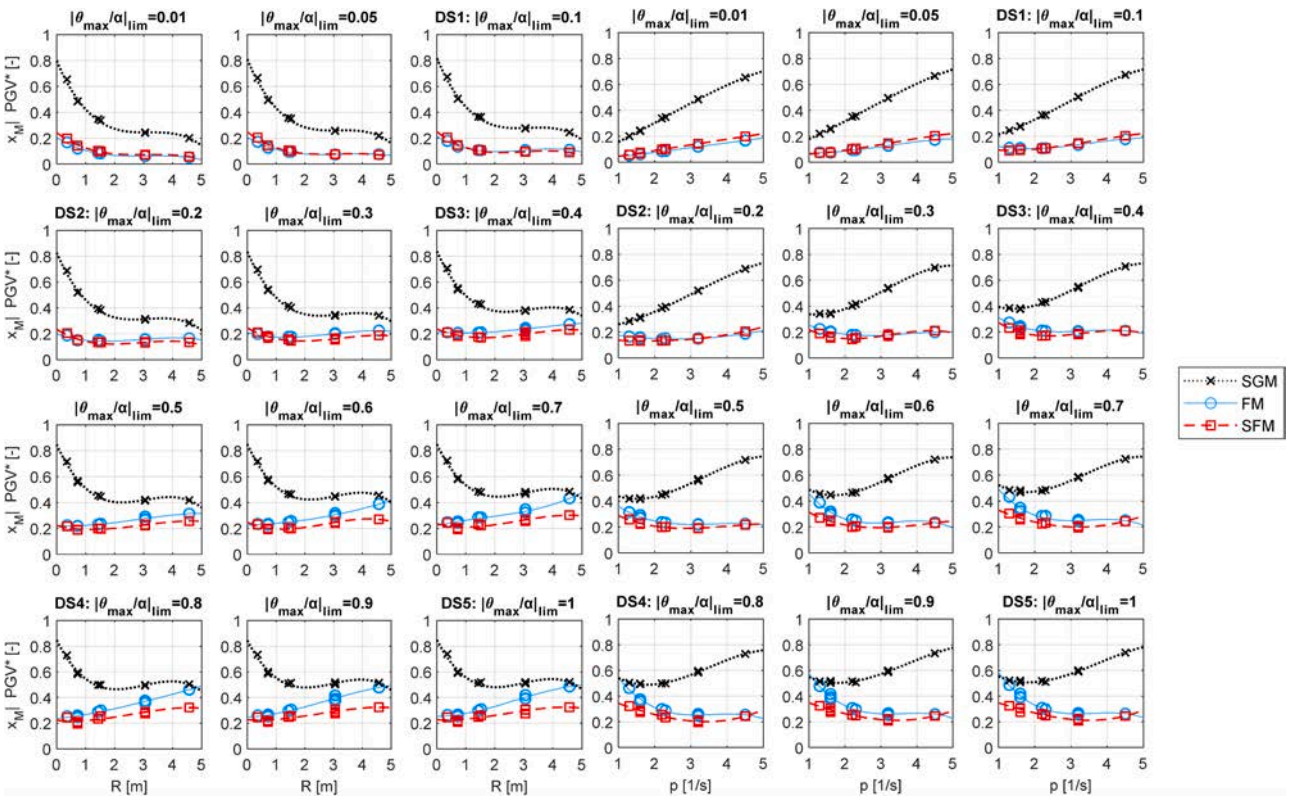

Fig. 6. Capacity curves (fragility medians (x_M)), expressed in terms of dimensionless peak ground velocity (PGV*) associated with rigid blocks (RBs), as a function of semi-diagonal block dimension (R) or frequency parameter (p), for the investigated DSs, considering strong ground motion (SGM), floor motion (FM), and strong floor motion (SFM) sets.

capacity surfaces were developed by fitting the capacities in three dimensions, i.e., PGA* or PGV*, $|\theta_{max}/\alpha|_{lim}$, and R or p. The fitting was implemented through second-degree polynomial correlations for all investigated cases, and COD was significantly high in all cases (e.g., larger than 0.9). Fig. 7 shows (a) an example of 3D view of capacity surface and (b) all relevant 2D views of capacity surfaces, considering the fragility median (x_M) of PGA* and PGV*, expressed as a function of $|\theta_{max}/\alpha|_{lim}$ and R or p, for SGM, FM, and SFM sets. The formulation of the fitting surface is reported in Eq. (10), where Z represents IMs PGA* or PGV*, X corresponds to $|\theta_{max}/\alpha|_{lim}$, and Z stands for DPs R or p. Fitting coefficients and related COD values are reported in the Appendix.

$$x_M|Z = S_{00} + S_{10}X + S_{01}Y + S_{20}X^2 + S_{11}XY + S_{02}Y^2 \quad (10)$$

The high quality of the fitting, which could be visually assessed considering the two example of 3D views (Fig. 6a) and quantitatively measured through COD values (ranging in 0.92 – 0.99, see Appendix), together with the consistency of the identified tendencies, proves that the capacity of rigid blocks is very well correlated to the combination of limit dimensionless rocking amplitude and geometric/dynamic parameters of the blocks. The comparison among the 2D views depicted in Fig. 6 clearly shows the relationship between the different input sets and investigated IMs. The median capacity associated with rigid blocks can be efficiently estimated by closed-form formulations, despite the dynamic response of rigid blocks is extremely complex and heavily nonlinear. The provided surfaces represent capacity estimation tools that are "universal" in the sense that was defined in [37], where the same formulation and different coefficients can express the different IMs and input sets, as a function of the block geometry/dynamic parameters (R and p). Further comments are omitted since the surfaces finalize the insights already discussed with regard to the previous figures, providing clear, quantitative, and robust criteria that are widely extendable and that could also be referred to for practical purposes (e.g., design and assessment of unanchored structural and nonstructural elements in the practice).

4.2. Single-degree-of-freedom systems

4.2.1. Methodology

The seismic capacity associated with the case study SDOF systems was assessed by processing the results of a recent study carried out by the authors [58]. The seismic response and capacity were estimated by performing incremental dynamic analyses in OpenSees [107], implementing lumped plasticity modeling of SDOF systems. The elastic-plastic response of the SDOF elements was modeled through the series of (a) a *zerolength* elastic-plastic spring, defined between the fixed (base) node (node 1) and an internal node (node 100) and (b) a linearly elastic monodimensional element, defined between the abovementioned internal node (node 100) and the free end node (node 2), where the lumped mass was applied; the series system is depicted in Fig. 8a. The structural model was developed implementing the Ibarra-Medina-Krawinkler (IMK) model [108], assigning the *UniaxialMaterial ModIMKPeakOriented* material [109] to the spring; the moment-rotation backbone response and the degradation parameters are depicted in Fig. 8b.

The elastic parameters were computed according to the cross-sectional properties. The inelastic rotation capacities and the cyclic degradation parameter were derived from the formulations developed by Lignos and Krawinkler [109,110], expressing the abovementioned features as a function of three dimensionless components: cross-sectional component, applied to yielding axial force ratio, and material component, as it is reported in Eq. (11), where $\overline{X}$ represents the parameter to assess (inelastic rotation capacities and cyclic degradation parameter), and N, N_y, σ_y, and C are applied axial force, yielding axial force, yielding strength, and stress strength conversion coefficient,

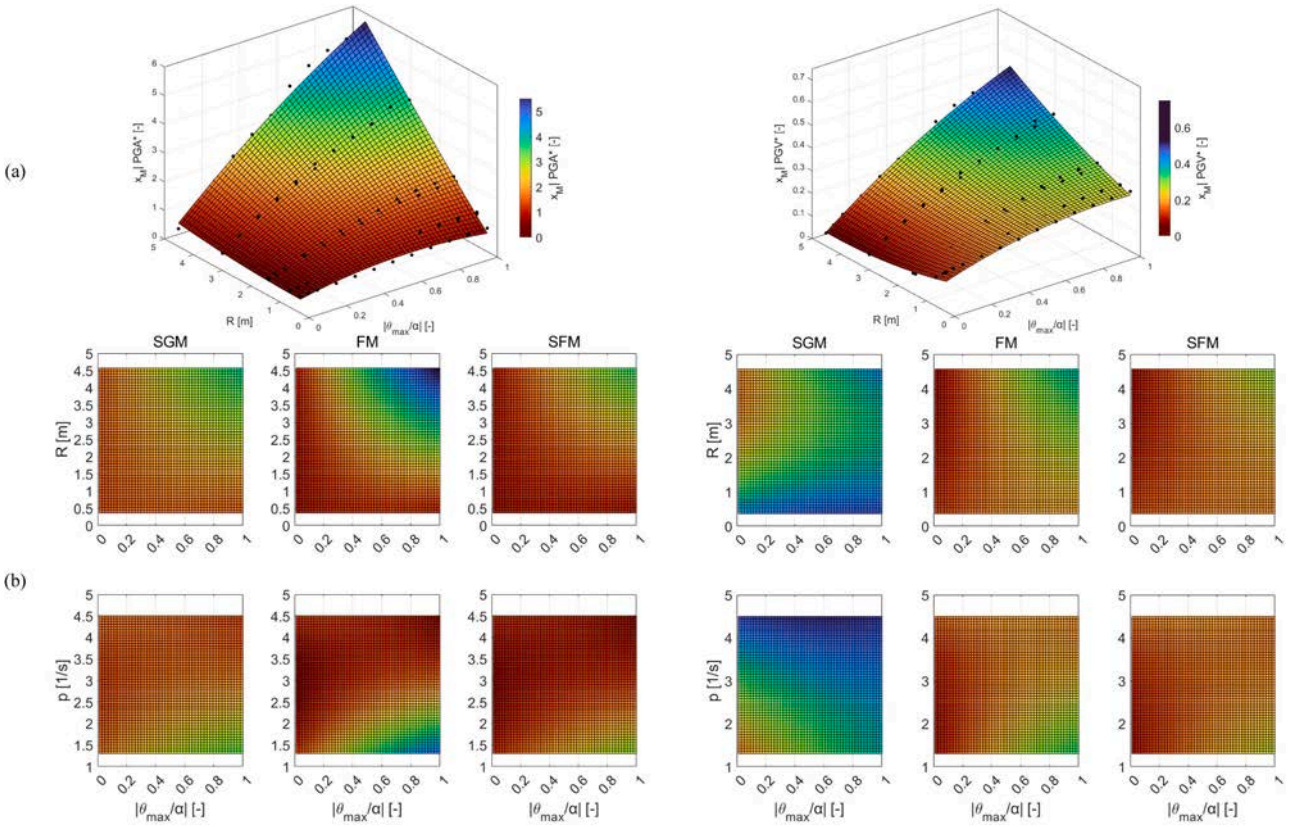

Fig. 7. (a) 3D view (FM set, function of R) and (b) 2D view capacity surfaces (fragility medians (x_M)) associated with rigid blocks (RBs), expressed in terms of dimensionless peak ground acceleration (PGA*) and dimensionless peak ground velocity (PGV*), as a function of limit dimensionless rocking amplitude angle ($|\theta_{max}/\alpha|_{lim}$) and semi-diagonal block dimension (R) or frequency block parameter (p), considering strong ground motion (SGM), floor motion (FM), and strong floor motion (SFM) sets.

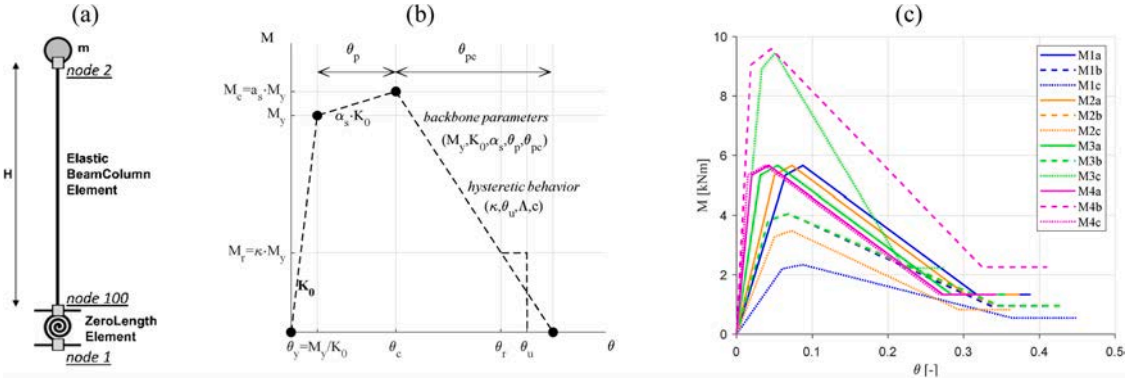

Fig. 8. Numerical modeling [58]: (a) series model, (b) Ibarra-Medina-Krawinkler (IMK) backbone and hysteretic/degradation parameters [108], and (c) backbone response of the investigated models.

respectively; a, b, c, and d are empirical coefficients, provided as a function of the parameter to assess [110].

$$\overline{X} = a\left(\frac{b}{t}\right)^{b}\left(1-\frac{N}{N_y}\right)^{c}\left(\frac{C\cdot\sigma_y}{380}\right)^{d} \tag{11}$$

Rayleigh damping (5 % damping ratio) was assigned to the elastic elements; P-Δ effects, namely second-order geometric nonlinearities, were accounted for. Incremental analyses were carried out by considering PFA as an IM and (lateral) mass displacement Δ as a DM, considering both ground and floor motions as loading histories. Two sets of floor motions were considered as analysis inputs: the first set consists in FM set used for RB analysis (as described in Section 4.1.1; Fig. 2) without six inputs; these inputs, namely FMs #4, #8, #11, #16, #20, and #24 as defined in D'Angela et al. [38], were found to be extremely mild with regard to the case study models in a pilot study. The resulting FM set includes a number of 18 records, and comprises an equal number of FF and NF records, as well as it was equally representative of low-, medium-, and high-rise buildings, as discussed in D'Angela et al. [58]. The second floor motion set coincided with the strong floor motion set defined in Section 4.1.1, i.e., namely SFM set.

The capacity curves were estimated as it was described regarding RBs (Section 4.1.1), considering both PGA and PGV, since both IMs were expected to be correlated to the seismic response of SDOF elements. DS occurring was associated with Eq. (8), where DM_{dyn} is $|\Delta_{max}|$ associated

with the dynamic analyses and DM_{lim} is $|\Delta_{max}|_{lim}$, i.e., the DS DM capacity limit threshold. Five DSs and corresponding $|\Delta_{max}|_{lim}$ thresholds were defined by identifying: (DS1) half yielding displacement or strength, (DS2) yielding displacement or strength, (DS3) capping strength displacement, (DS4) 20 % drop in strength (after capping strength) displacement, and (DS5) onset of perfectly plastic response displacement or residual strength achievement. The related capacity thresholds were defined according to the nonlinear static (pushover) response of SDOF elements including P-Δ effects. The limit dimensionless displacement $|\Delta_{max}|_{lim}/|\Delta_{max}|_{DS5}$ was considered for the elaboration of the capacity curves and surfaces, where $|\Delta_{max}|_{DS5}$ is the DS DM capacity limit threshold associated with DS5; this condition was applied for the sake of comparison among the investigated models (the derived DM is dimensionless and maximum value is equal to unity for all models).

Fig. 9 shows the ductility capacity (μ) of the investigated models, defined as ratio between DS3, DS4 and DS5 displacement capacities and yielding displacement, corresponding to DS2. Mean μ associated with DS3, DS4, and DS5 capacity are equal to 1.75, 3.42, and 8.41, respectively, and the coefficient of variation is equal to 22.8 %, 43,8 %, and 57.1 %, respectively. It should be recalled that these ductility measures derive from the implemented response formulation, as it was described above. μ values related to DS3 range within 1.3–2.5, and μ values related to DS4 associated with (a) all models but M4 and (b) all models mean range within 2–3.5; these values are compatible with literature assumptions/ranges [47,49]. M4 models present μ related to DS4 in the order of 6, assuming higher ductility capacities. DS5 μ are twice or more than DS4 ones, due to the low-slope degradation model. For the investigated element type, μ values and data dispersion tend to increase as elastic frequency increases, and ductility ratios within the same group do not significantly vary.

The capacity curves and surfaces associated with SDOF elements were assessed as it was done for RBs, i.e., considering FPs. In particular, x_M values were fitted as a function of SDOF geometry and frequency-based parameters, considering PGA and PGV, for both FM sets; the results were elaborated considering f_a as a key DP since this latter parameter was found to be well correlated to the SDOF results, also considering the inelastic response. The quality of the fitting was assessed by COD, which resulted in high values in several cases. The resulting correlations and related COD values are reported in the Appendix. The σ values were also fitted as it was done for x_M considering second-degree polynomial equations, resulting in high COD values in several cases. However, the results are not depicted since the focus of the present study is on the capacity, but all fitted correlations and related COD values are reported in the Appendix.

4.2.2. Results

Figs. 10 and 11 depict x_M and σ, respectively, as a function of $|\Delta_{max}|_{lim}/|\Delta_{max}|_{DS5}$. The curves report the fragility parameters as a function of DSs, equivalent to achievement of $|\Delta_{max}|_{lim}/|\Delta_{max}|_{DS5}$ thresholds, corresponding to the markers. The x_M curves (Fig. 10) associated with PGV represent the PGA curves scaled by the PGA/PGV ratio related to the relevant set (they show median values), and, therefore, only PGA curves are discussed in the following, and the reader is referred to Fig. 10 for quantitative interpretation of PGV curves. Differently, the curves expressing σ (Fig. 11) account for the uncertainty associated with PGV to PGA distribution and differ for PGA and PGV.

Concerning x_M and PGA (Fig. 10), it is interesting to notice that the segments that connect the subsequent markers tend to decrease in slope in a consistent manner: the multi-linear curves associated with the subsequent segments depict relatively stable behavior as $|\Delta_{max}|_{lim}/|\Delta_{max}|_{DS5}$ grows, interpreting the evolution of the dynamic capacities over the increase of damage and nonlinearity, or, more generally, dimensionless deformation conditions. The initial branches of the curves, defined between null $|\Delta_{max}|_{lim}/|\Delta_{max}|_{DS5}$ values and yielding conditions (second $|\Delta_{max}|_{lim}/|\Delta_{max}|_{DS5}$ threshold), represent an elastic measure of dynamic stiffness, expressed as an IM capacity variation over $|\Delta_{max}|_{lim}/|\Delta_{max}|_{DS5}$ variation, and this obviously reflects the elastic properties of the models; for example, see the backbone initial slopes in Fig. 8c. However, the deformation metrics used in Fig. 10 refer to the newly defined dimensionless displacement and it cannot be simply associated with the backbone response plotted in Fig. 8c; for example, the same elastic stiffness expressed in Fig. 8c would differ in Fig. 10 from two models that have different $|\Delta_{max}|_{DS5}$ values. However, the considered metrics allow to quantify the capacities directly accounting for nonlinear evolution of the behavior and considering a derived measure of ductility. Curves depicted in Fig. 10 are extremely useful for estimating the nonlinear behavior of the investigated model, meant as a nonlinear dynamic capacity curves; furthermore, these describe a median response, expressed as a function of the different floor motion sets, namely FM and SFM. It is clear the overall higher severity of SFM set, associated with lower capacity curves, compared to FM set. The higher severity is more significant as the nonlinear response evolves: there are minor differences over the elastic responses, whereas the discrepancy between FM and SFM significantly increases as the nonlinearity evolves.

The evolution of σ as a function of $|\Delta_{max}|_{lim}/|\Delta_{max}|_{DS5}$ (Fig. 11) quantitatively defines the influence of the nonlinearity on the uncertainty associated with the SDOF capacities, also reflecting the different trends associated with different IMs and floor motion sets. Considering PGA and FM, σ essentially only depends on the elastic frequency, as, for the different model groups, σ is overall constant as $|\Delta_{max}|_{lim}/|\Delta_{max}|_{DS5}$ grows, with minor oscillations, mostly associated with few models. σ tends to decrease as the stiffness of the models increases: M1 group is associated with the highest uncertainty with a minor influence of the model characteristics other than frequency, ranging within 0.9 and 1; σ related to M2 group has an even lower influence of the models features other than the elastic frequency, and it is associated with σ just lower than model M1 group one (ranging within 0.8–0.9). M3 group is associated with an approximately null dispersion due to the models features other than the elastic frequency for all DSs but DS5 achievement, and the overall σ ranges in 0.6–0.7.

M4 group is associated with the lowest uncertainty, which differs

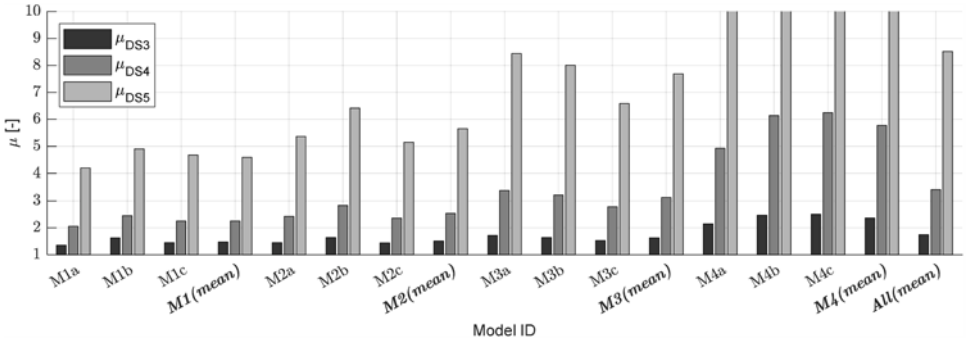

Fig. 9. SDOF elements model ductility (μ) referred to DS3, DS4, and DS5 conditions.

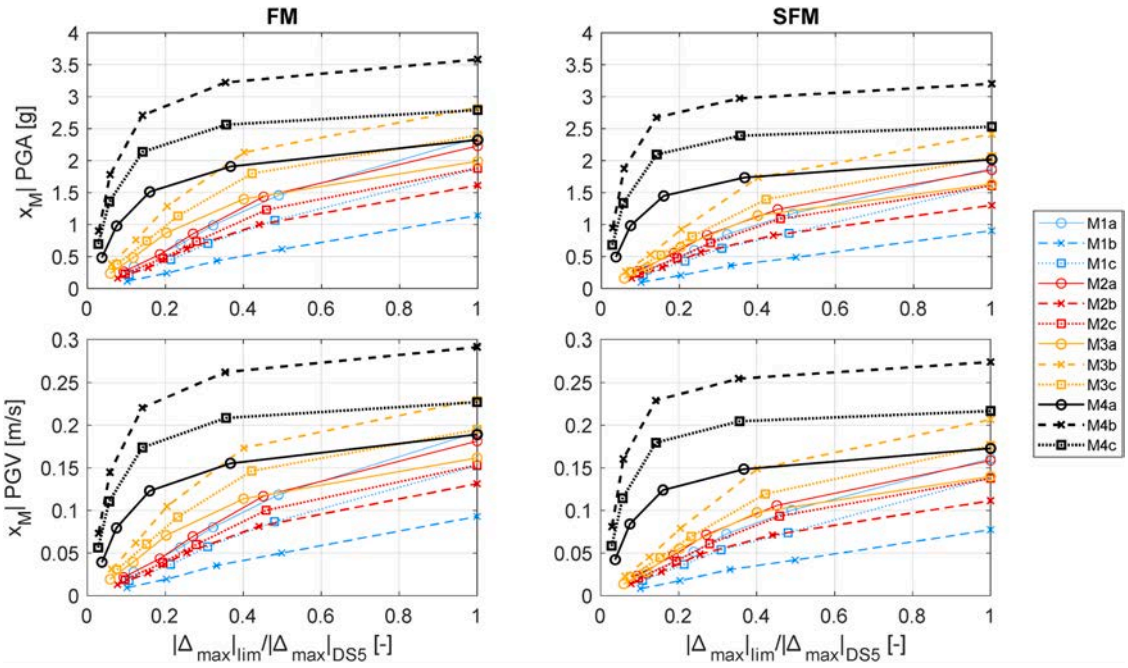

Fig. 10. Fragility median (x_M) in terms of peak ground acceleration (PGA) and peak ground velocity (PGV) associated with single-degree-of-freedom (SDOF) systems, as a function of limit dimensionless displacement $|\Delta_{max}|_{lim}/|\Delta_{max}|_{DS5}$, considering floor motion (FM) and strong floor motion (SFM) sets.

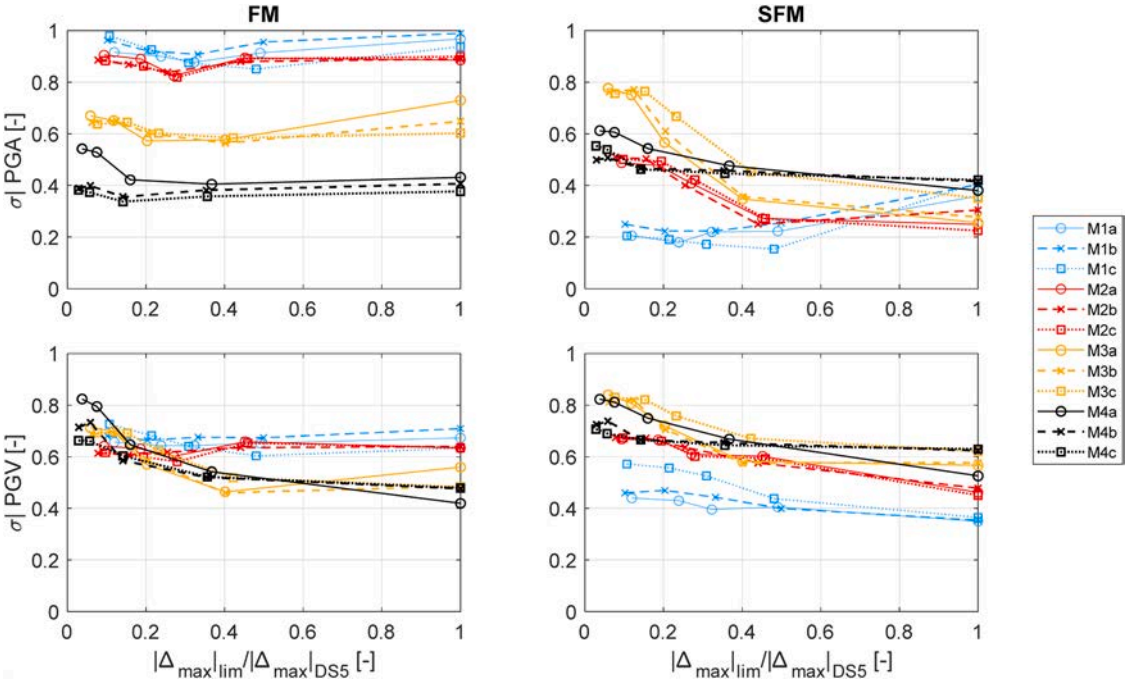

Fig. 11. Fragility logarithmic standard deviation (σ) in terms of peak ground acceleration (PGA) and peak ground velocity (PGV) associated with single-degree-of-freedom (SDOF) systems, as a function of limit dimensionless displacement $|\Delta_{max}|_{lim}/|\Delta_{max}|_{DS5}$, considering floor motion (FM) and strong floor motion (SFM) sets.

more among the M4 models over the elastic response, tending to converge for higher damage conditions; σ related to M4 group ranges within 0.35–0.55, but the behavior is more appropriately associated with about 0.4. The abovementioned findings show that the response uncertainty is not conditioned by the nonlinearity, at least considering FM set, which is representative of low- to high-intensity signals. The trend associated with SFM set is different from the one related to FM set. In particular, it is interesting to notice that, for all model groups but M1 one, as $|\Delta_{max}|_{lim}/|\Delta_{max}|_{DS5}$ increases, the uncertainty tends to decrease and the σ value associated with the most severe damage condition (DS5) does not significantly depend on the model characteristics, including the frequency. Overall, the highest uncertainty is associated with M3 models over the elastic response (σ is just lower than 0.8), whereas for models M2 and M4, the highest uncertainty, still associated with the elastic response, is approximately within 0.5–0.6. The most deformable models, i.e., M1 group ones, are associated with an uncertainty that tends to increase as $|\Delta_{max}|_{lim}/|\Delta_{max}|_{DS5}$ grows, with σ values that are significantly lower than other models' ones over the elastic response; M1

group σ is more compatible with other models over more severe damage conditions, especially, corresponding to DS5.

Considering PGV, the uncertainty responses associated with FM and SFM sets are relatively similar, in terms of tendencies: σ overall tends to decrease as $|\Delta_{max}|_{lim}/|\Delta_{max}|_{DS5}$ increases for all models. The influence of the model frequency related to FM PGV is significantly less relevant than FM PGA one: for all models, the highest σ related to FM PGV is associated with the elastic response and is quite similar among all models (within 0.65–0.8), and σ tends to decrease slightly increasing the model-to-model dispersion for higher damage severity conditions, showing σ values ranging from 0.4 to 0.7 corresponding to DS5. Comparing PGA and PGV responses, considering FM set, it can be noted that PGV can be more efficient than PGA (a) for relatively deformable models (M1 and M2 models) over the whole damage condition evolution and (b) for moderately stiff models (M3 models) for moderate to severe damage conditions; conversely, PGA is more efficient than PGV for highly stiff models (M4 models), over the whole damage condition evolution but collapse condition, for which PGA and PGV correspond to similar uncertainty (and efficiency). Considering SFM, σ evolution is more similar to FM one for PGV, even though some differences can be identified. In particular, models M1 are associated with lower σ values for SFM (within 0.4–0.6), whereas models M3 and M4 provide higher σ values, especially over the nonlinear response; for SFM set, models M2 are associated with σ values (lower) higher over the (nonlinear) elastic response. The range of σ associated with collapse related to SFM set is relatively similar to FM set one, even though, as previously described, models M1 provide the lowest σ value (lower than 0.4), and models M3 and M4 are associated with the highest σ value (between 0.55 and 0.65); this latter trend is opposite to the one associated with FM set response.

Fig. 12 shows the capacity curves considering both PGA and PGV,

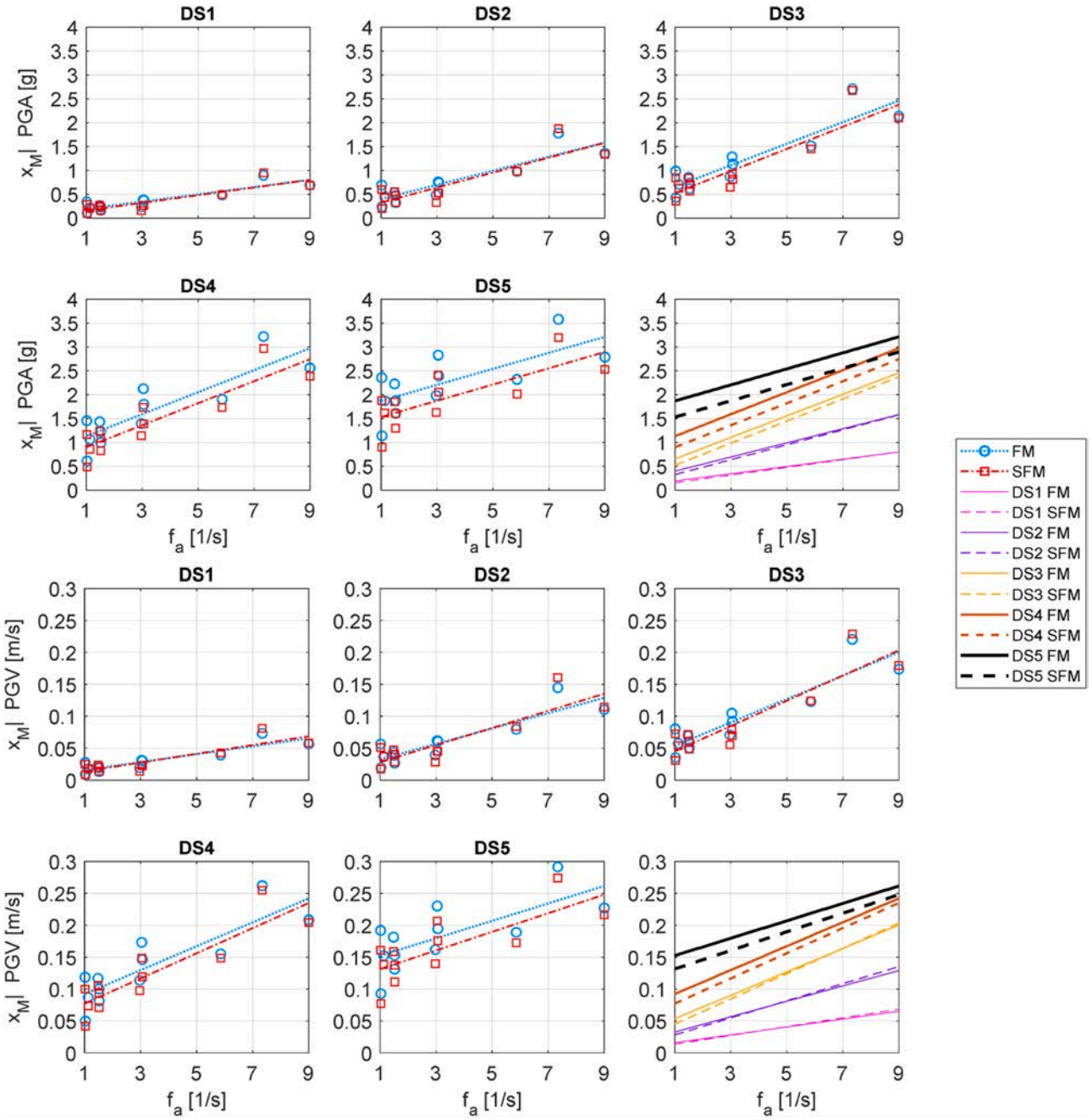

Fig. 12. Capacity curves (fragility medians (x_M)), expressed in terms of peak ground acceleration (PGA) and peak ground velocity (PGV) associated with single-degree-of-freedom (SDOF) systems, as a function of SDOF frequency (f_a), for the investigated DSs, considering floor motion (FM) and strong floor motion (SFM) sets.

expressed as fitting x_M vs. f_a curves, considering FM and SFM sets. For both PGA and PGV, the influence of the floor motion set is null over the elastic DSs (DS1 and DS2), and considering the capping condition (DS3), the influence is minor for PGA and approximately null for PGV. For higher DS conditions, i.e., 20 % strength drop (DS4) and collapse (DS5), SFM set is more severe than FM one, and the SFM to FM capacity difference is larger for DS5 than for DS4. The slope of the fitting curves and the line intercept tend to increase as the damage condition evolves from DS1 to DS3 for both PGA and PGV, whereas passing from DS3 to DS4, the slope is approximately the same and the intercept increases. Finally, passing from DS4 to DS5, the slope tends to decrease and the intercept grows. All fitting coefficients and related COD are reported in the Appendix. For both FM and SFM sets, PGA and PGV COD ranges in 0.74–0.83 over DS1 to DS4, whereas this is lower for DS5, corresponding to about 0.51 for FM set and 0.59 for SFM. The expression of FP is reported in Eq. (12), where FP relates to x_M or σ, IM corresponds to PGA or PGV, and DP refers to f_a; fitting coefficients and related COD are reported in the Appendix

$$FP|IM = C_{11}DP + C_{12} \tag{12}$$

The capacity surfaces shown in Fig. 13 synthetize the clear correlation between the SDOF capacity (x_M) and the key parameters associated with dynamic properties of SDOF elements (f_a) and damage severity ($|\Delta_{max}|_{lim}/|\Delta_{max}|_{DS5}$). The formulation of the fitting surface is reported in Eq. (13), where Z corresponds to IMs PGA or PGV, X to DP f_a, and Y to $|\Delta_{max}|_{lim}/|\Delta_{max}|_{DS5}$; fitting coefficients and related COD values are reported in the Appendix.

$$x_M|Z = S_{00} + S_{10}X + S_{01}Y + S_{11}XY + S_{02}Y^2 \tag{13}$$

The fitted surfaces are associated with high COD values, equal to about 0.84 and 0.82 corresponding to FM and SFM sets, respectively, as reported in the Appendix. Comparing FM and SFM capacity surfaces allows to clearly identify the parameter ranges in which SFM set is more severe than FM one, i.e., higher $|\Delta_{max}|_{lim}/|\Delta_{max}|_{DS5}$ and lower f_a, as it was already qualitative discussed regarding the capacity curves shown in Fig. 12. The surfaces provided can be easily used to expeditiously estimate the seismic capacity of a wide range of inelastic SDOF, accounting for elastic frequency and inelastic response. Further comments are omitted for the sake of brevity, and the reader is referred to the Appendix for quantitative remarks.

The study accounts for a wide range of building and NE scenarios, and these latter also include cases of significant sensitivity of nonstructural elements to building properties (e.g., resonance conditions). As a matter of fact, both nonstructural elements and buildings vary their period within a wide range of cases. This condition can be confirmed referring to [54], where the acceleration component amplification factors of the investigated SDOF elements were estimated. Under the investigated floor motions, these factors reach values larger than 4 in several cases, and, in few cases, even significantly larger values. Therefore, NE to structural resonance phenomena, which are known to be extremely severe on acceleration amplifications [45], are considered in terms of record-to-record uncertainty (or building period variation) and in terms of relation between the elastic frequency and the expected building period. In conclusion, the study does not directly address the resonance phenomena, but dataset includes resonance conditions, and the paper provides the tools to account for them, when expected, in a simplified but reasonable manner.

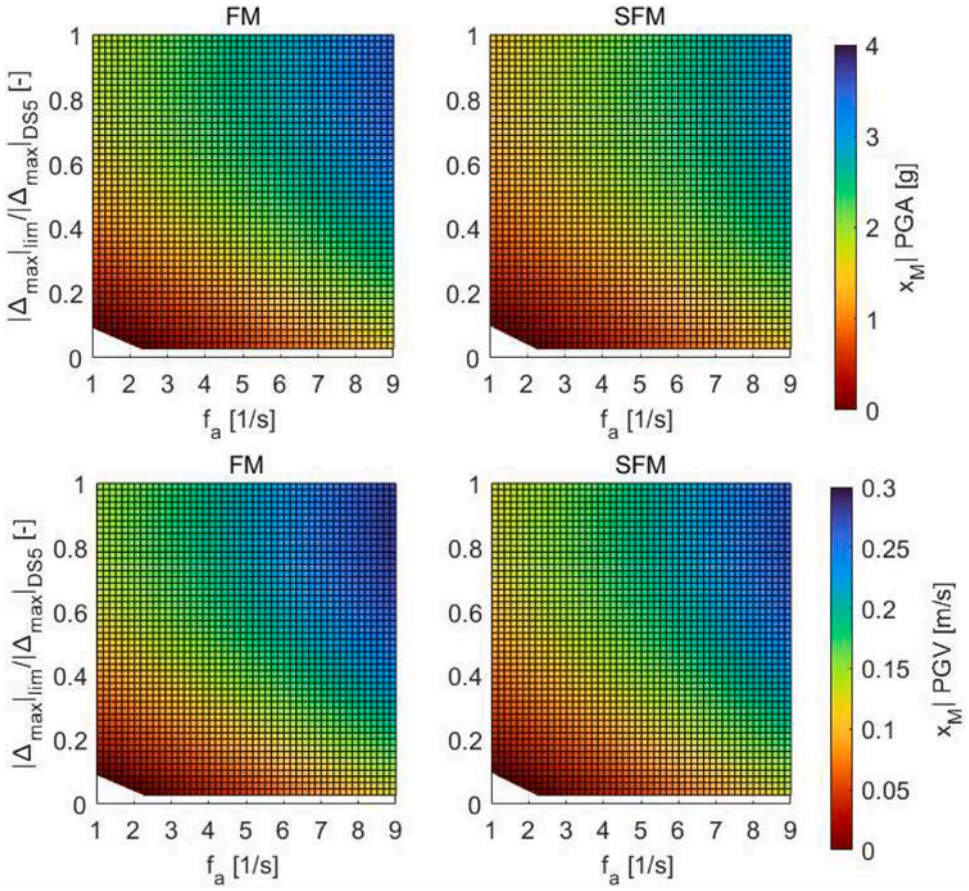

Fig. 13. 2D view capacity surfaces (fragility medians (x_M)) associated with single-degree-of-freedom (SDOF) systems, expressed in terms of peak ground acceleration (PGA) and peak ground velocity (PGV), as a function of limit dimensionless displacement $|\Delta_{max}|_{lim}/|\Delta_{max}|_{DS5}$ and SDOF frequency (f_a), considering floor motion (FM) and strong floor motion (SFM) sets.

5. Safety assessment

PLs and LSs defined in Section 3.3 were quantitatively associated with DSs for both RBs and SDOF elements. In particular, PL1, PL2, and PL3 were performed through OLS, DLS, and LSLS verifications, respectively, accounting for DS1, DS2, and DS3, respectively, according to the definition of DSs related to RBs and SDOF, discussed in Sections 4.1.1 and 4.2.1, respectively. It should be noted that safety assessment associated with LSLS conservatively assumes a ductility capacity ranging from 1.3 to 2.5, as it is discussed with regard to DS3 ductility ratios depicted in Fig. 9. Therefore, the safety assessment results should be referred to in case the abovementioned ductility levels are guaranteed by NEs of interest. Figs. 14 and 15 shows the seismic safety assessment results for RBs (SDOF systems), considering PGA* and PGV* (PGA and PGV), for ordinary and critical buildings, associated with L'Aquila and Naples sites. For SDOF elements, the safety conditions were expressed as a function of both mass (m) and elastic frequency (f_a). The cases related to Milan do not exhibit unsafe conditions for both RBs and SDOF systems; the abovementioned trivial cases are not depicted in the paper. A tabular comparison among the meaningful safety results is reported in Table 4 regarding RBs and SDOF systems, also accounting for PFA. It is recalled that the safety assessment was performed considering median capacities (Section 4) and seismic demands provided by the Italian building code (Section 3).

Regarding RBs (Fig. 14 and Table 4), the most critical cases, i.e., associated with unsafe conditions, are associated with higher h/b ratio, and, in some cases, with lower R, majorly depending on site (L'Aquila and Naples), building importance class (ordinary and critical buildings), considered LSs (OLS, DLS, and LSLS), and input type (SGM, FM, and SFM sets), and minorly on IM (PGA, PGV, and PFA). According to Fig. 14, in case of high seismicity (L'Aquila site), most equipment and contents housed at top floors of critical facilities (e.g., NEs having $R < 2$ m and $h/b > 2$) are likely to be unsafe for the three investigated LSs, especially for DLS and LSLS; the safety conditions are less critical but still potentially concerning for item and equipment located at the ground floors of critical buildings, especially for LSLS verification. Considering moderate seismicity (Naples site), the safety condition of abovementioned elements is also critical, especially for elements installed at top floors, for all considered LSs. For ordinary buildings, LSLS is still critical and extremely critical for elements located at the ground and top floor of buildings, respectively, for high-seismicity sites, whereas, for moderate-seismicity sites, LSLS is critical only considering elements located at top building floors. For high-seismicity sites, OLS and DLS are critical only if the elements are located at the top building floors, whereas no concern is related to elements that are at the ground floor. Considering moderate seismicity, OLS and DLS are not associated with concerning safety conditions, unless very slender elements located at top building floors are considered for DLS. In Fig. 14 and Table 4, it is interesting to note that there is often a correspondence between the safety estimations associated with the different IMs, and the following remarks can be identified. PGV is slightly more severe than PGA (and PFA) for detecting the unsafety conditions, whereas PFA, meant as an EDP, is overall slightly less severe than PGA (and PGV); more quantitative remarks can be derived from Table 4, but further comments are omitted for the sake of brevity. The overall consistency among PGA, PGV, and PFA confirms that capacity and demand correlations among the investigated IMs and EDP are compatible among them. However, the findings stress the need for performing safety assessment considering multiple parameters, for example, possibly, combining IM, EDP, and DM.

Concerning SDOF elements (Fig. 15 and Table 4), the safety assessment is significantly less critical than the one associated with RBs. Overall, ordinary facilities are not associated with unsafe conditions, unless very few cases are considered, i.e., low frequency and high mass conditions for OLS verification at high-seismicity sites (L'Aquila) for

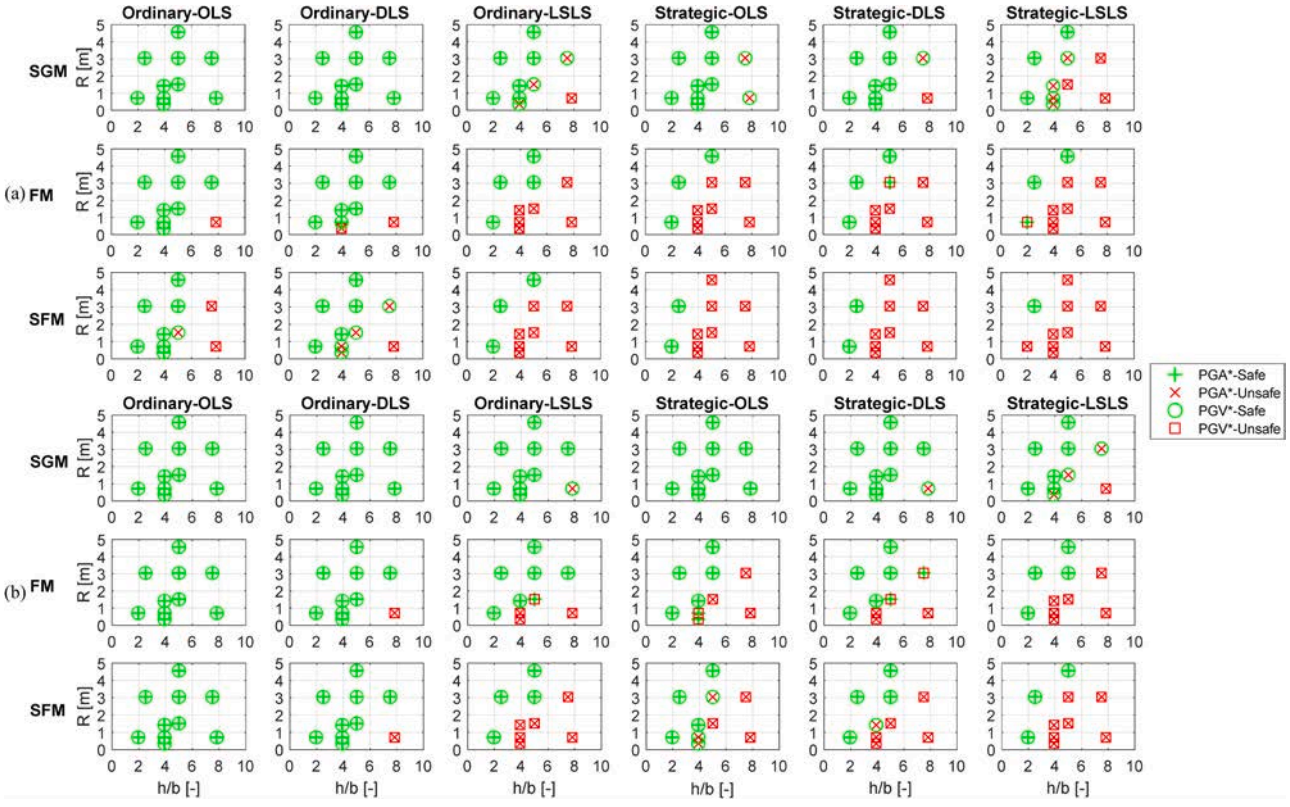

Fig. 14. Seismic safety assessment results for rigid blocks (RBs), considering dimensionless peak ground acceleration (PGA*) and dimensionless peak ground velocity (PGV*), for ordinary and critical buildings, and operativity limit state, (OLS), damage limitation limit state (DLS), and life safety limit state (LSLS), considering (a) L'Aquila and (b) Naples.

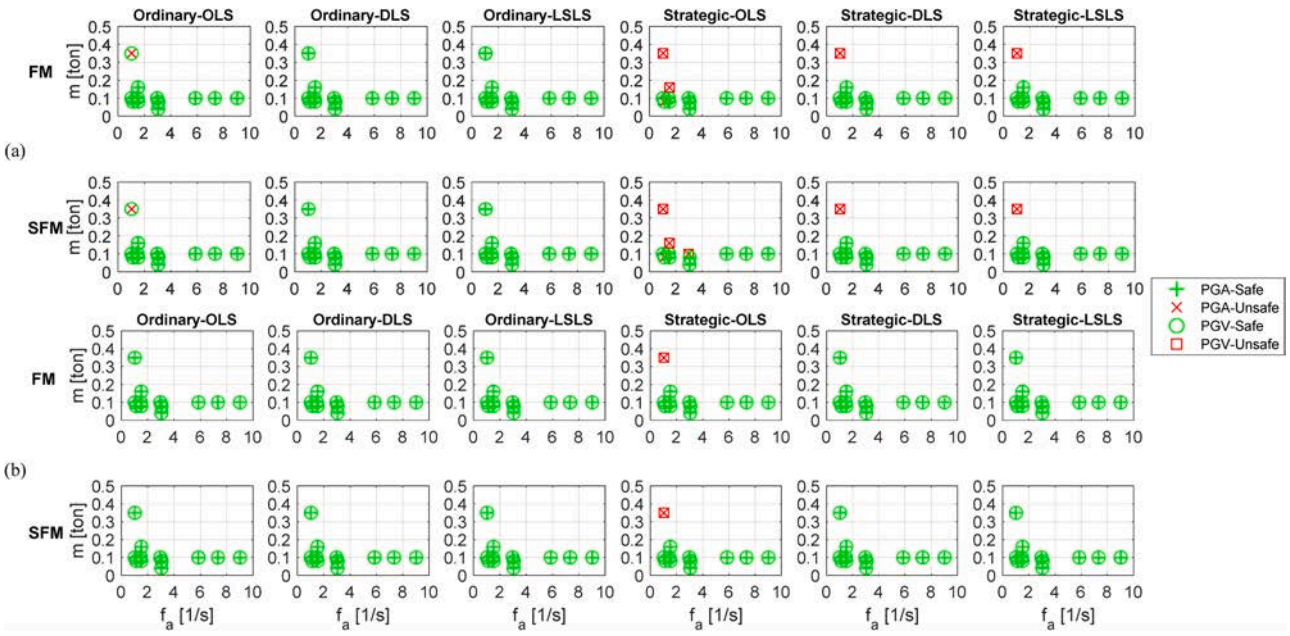

Fig. 15. Seismic safety assessment results for single-degree-of-freedom (SDOF) systems considering peak ground acceleration (PGA) and peak ground velocity (PGV), for ordinary and critical buildings, and operativity limit state, (OLS), damage limitation limit state (DLS), and life safety limit state (LSLS), considering (a) L'Aquila and (b) Naples.

Table 4
Seismic safety assessment results for rigid blocks (RBs) and single-degree-of-freedom (SDOF) systems, considering peak floor acceleration (PFA), peak ground acceleration (PGA) and peak ground velocity (PGV) as an intensity measure (IM), for ordinary and critical buildings, and L'Aquila (AQ) and Naples (NA). OLS, DLS, and LSLS represent operativity limit state, damage limitation limit state, and life safety limit state, respectively.

SITES	BUILDING IMPORT. CLASS	LS	RB ID	#1A			#1B			#1C			#1D			#1E			#2A			#2B			#2C			#2D			#2E		
				PFA	PGA	PGV	PFA	PGA	PGV	PFA	PGA	PGV	PFA	PGA	PGV	PFA	PGA	PGV	PFA	PGA	PGV	PFA	PGA	PGV	PFA	PGA	PGV	PFA	PGA	PGV	PFA	PGA	PGV
AQ	Ord.	OSL →		V	V	V	V	V	V	V	V	V	X	X	X	V	V	V	V	V	V	V	V	V	V	V	V	V	V	V	V	V	V
		DLS →		V	X	X	V	V	V	V	V	V	X	X	X	V	V	V	V	V	V	V	V	V	V	V	V	V	V	V	V	V	V
		LSLS →		X	X	X	V	V	V	X	X	X	X	X	X	V	X	X	X	X	X	V	V	V	V	V	V	X	X	X	V	V	V
	Crit.	OSL →		X	X	X	V	V	V	X	X	X	X	X	X	X	X	X	X	X	X	V	V	V	X	X	X	X	X	X	V	V	V
		DLS →		X	X	X	V	V	V	X	X	X	X	X	X	V	X	X	X	X	X	V	V	V	V	V	X	X	X	X	V	V	V
		LSLS →		X	X	X	V	V	X	X	X	X	X	X	X	X	X	X	X	X	X	V	V	V	V	X	X	X	X	X	V	V	V
NA	Ord.	OSL →		V	V	V	V	V	V	V	V	V	V	V	V	V	V	V	V	V	V	V	V	V	V	V	V	V	V	V	V	V	V
		DLS →		V	V	V	V	V	V	V	V	V	V	X	X	V	V	V	V	V	V	V	V	V	V	V	V	V	V	V	V	V	V
		LSLS →		X	X	X	V	V	V	V	X	X	X	X	X	V	V	V	V	V	X	V	V	V	V	V	V	V	V	V	V	V	V
	Crit.	OSL →		V	V	X	V	V	V	V	V	X	X	X	X	V	V	V	V	X	X	V	V	V	V	V	V	V	X	X	V	V	V
		DLS →		X	X	X	V	V	V	V	X	X	X	X	X	V	V	V	V	V	X	V	V	V	V	V	V	V	V	X	V	V	V
		LSLS →		X	X	X	V	V	V	X	X	X	X	X	X	V	X	X	X	X	X	V	V	V	V	V	V	X	X	X	V	V	V

SITES	BUILDING IMPORT. CLASS	LS	SDOF ID	M1B			M1C			M2B		
				PFA	PGA	PGV	PFA	PGA	PGV	PFA	PGA	PGV
AQ	Crit.	OSL →		X	X	X	V	X	V	X	X	X
		DLS →		X	X	X	V	V	V	V	V	V
		LSLS →		V	X	X	V	V	V	V	V	V
NA		OSL →		X	X	X	V	V	V	V	V	V
		DLS →		V	V	V	V	V	V	V	V	V
		LSLS →		V	V	V	V	V	V	V	V	V

V Safe X Unsafe

elements housed at the top building floors. For critical buildings, there are some critical cases for high-seismicity sites, associated with low frequencies for all LSs. One critical condition was identified for medium-seismicity sites (Naples) and critical buildings, related to OLS verification of low frequency and high mass conditions. Also, for SDOF elements, there is a clear correspondence among the investigated IMs (PGA

and PGV) and EDP (PFA). Only in two cases out of six, one or two parameters detect the unsafe conditions, whereas in all other cases all three parameters provide the same safety result. Once again, it is confirmed the consistency among the capacity and demand correlations that correlate the investigated IM and EDP. In all other cases, no critical safety conditions are detected, even though the study cannot be considered to be exhaustive and definitive.

6. Concluding remarks

The study provided methodological guidance and quantitative metrics associated with seismic capacity assessment and safety measures. Numerical analyses were carried out considering rigid blocks (RBs) and inelastic single-degree-of-freedom (SDOF) elements as nonstructural elements (NEs). Seismic demand was assessed according to the Italian building code, considering the influence of the building, and seismic capacities were estimated by processing the results of the numerical analyses by means of an innovative methodology. The following original contributions have been made.

- A comprehensive methodological framework has been defined, by critically analyzing existing codes and literature studies, developing a novel technical synthesis that represents a systematic guideline; the correlations between the performance levels (PLs), limit states (LSs), damage states (DSs), damage measures (DMs), engineering demand parameters (EDPs), and intensity measures (IMs) have been discussed, referring to viable solutions for implementing the safety assessment methodology with regard to NEs. Scientific and technical/operative guidance and insights are provided, supporting the future implementation of the methodology in research studies, applications, or codes.
- The capacity assessment has been carried out following a robust and relatively simple methodology, considering unique metrics for different categories of NEs. The most significant methodological contribution concerning the case study NEs is associated with the development of the concept of statistical-based dynamic capacity curves and surfaces, which quantitatively correlate the seismic response and capacity of NEs to their geometric/dynamic parameters and to dimensionless DMs and DSs. For RBs, the concept of capacity curves and surfaces extends the concept of rocking and overturning spectra, whereas, for SDOF elements, it represents an novelty in the literature.
- The safety evaluation has been implemented considering a practical and reliable approach, which takes into account the uncertainty associated with record-to-record and building influence sources. The influence of multiple features and parameters have been considered for both RBs and inelastic SDOF systems: seismicity, building importance, input type (ground records and two sets of floor motions), geometric/dynamic properties, multiple assessment metrics and damage/nonlinearity measures. Applicable graphical and tabular tools have been developed for identification of potentially critical conditions of RBs and SDOF elements, and for the expeditious estimation of the seismic safety factors. The abovementioned criteria can be considered as a reference for design and assessment of acceleration-sensitive NEs that are compliant with RBs and inelastic SDOF systems, accounting for the variation of several parameters and for basic but representative uncertainty sources.

Whereas the developed methodology is widely applicable to different NE types and arrangements, the quantitative findings reflect the case study scenarios and NEs, and they should be applied to NEs that have a seismic behavior that is compatible with the implemented models. It is recalled that pure rocking behavior is assumed for RBs and no interaction with boundaries other than the support is accounted for. The capacities and safety assessment results related to SDOF systems reflect the modeling assumptions, with particular regard to the considered ductility capacities and to the simplified manner to account for nonstructural to structural resonance phenomena. Therefore, the provided results should be carefully considered for NEs with behavior and properties not compatible with the investigated scenarios. Further studies will extend the building scenarios and case studies, as well as consider further assessment parameters, such as further EDPs and DMs. As a final comment, it should be specified that the developed methodology is currently being applied for research purposes with regard to pilot healthcare facilities (PRIN 2020 ENRICH project) and it is also part of the course on healthcare building (Master's degree in Biomedical Engineering, University of Naples Federico II).

Funding and acknowledgments

The study was funded mainly by the Italian Ministry of University and Research (MUR) in the framework of PRIN 2020 project titled "ENRICH project: ENhancing the Resilience of Italian healthCare and Hospital facilities" and minorly by the Italian Department of Civil Protection (DPC) in the framework of the National project DPC – ReLUIS 2024-2026 WP17: "*Componenti non strutturali*". The technical and operative support of Dr. Martino Zito and Eng. Francesco Mario Calenzo are fully acknowledged. Finally, the Referees/Editors are thanked for Their insightful review/editorial comments as they have contributed to improving the quality and clarity of this work.

CRediT authorship contribution statement

Danilo D'Angela: Writing – review & editing, Writing – original draft, Visualization, Validation, Software, Methodology, Investigation, Formal analysis, Data curation, Conceptualization. **Gennaro Magliulo:** Writing – review & editing, Visualization, Validation, Supervision, Resources, Project administration, Methodology, Investigation, Funding acquisition, Formal analysis, Conceptualization.

Declaration of competing interest

The authors declare that they have no known competing financial interests or personal relationships that could have appeared to influence the work reported in this paper.

Appendix A

Tables A1–A15.

Table A1
Notation table.

Abbreviations	
AQ	L'Aquila site (Italy)
DLS	damage limitation limit state

(*continued on next page*)

Table A1 (*continued*)

Abbreviations	
DM	damage measure
DP	dynamic parameter
DS	damage state
EDP	engineering demand parameter
$EDP_{c,LS}$	EDP threshold value corresponding to the occurring of DS that is relevant to LS
$EDP_{d,LS}$	EDP threshold value corresponding to the seismic demand relevant to LS, compatible with DS of interest
FM	floor motion
FP	fragility parameter
GM	ground motion
HSS	hollow square steel section
IDR	interstory drift ratio
IM	intensity measure
IMK	Ibarra-Medina-Krawinkler model
LS	limit state
LSLS	life safety limit state
MI	Milan site (Italy)
NA	Naples site (Italy)
NCLS	near collapse limit state
NE	nonstructural elements
OLS	operativity limit state
PBEE	performance-based earthquake engineering
PL	performance level
P-Δ	second-order geometric nonlinearities
RB	rigid block
RC	reinforced concrete
RRS	required response spectrum
SDOF	single-degree-of-freedom
SFM	strong floor motion
SGM	strong ground motion
Symbols	
$\lvert\Delta_{max}\rvert$	SDOF (HSS) peak Δ (absolute value)
$\lvert\Delta_{max}\rvert_{DS}$	SDOF (HSS) peak Δ (absolute value) associated with DS
$\lvert\Delta_{max}\rvert_{lim}$	SDOF (HSS) Δ capacity (absolute value)
$\lvert\theta_{max}/\alpha\rvert$	dimensionless peak RB rotation (absolute value)
$\lvert\theta_{max}/\alpha\rvert_{lim}$	RB $\lvert\theta_{max}/\alpha\rvert$ capacity limit threshold (absolute value)
a,b,c,d	SDOF (HSS) empirical coefficients
a_g	seismic design acceleration at bedrock
b	RB semi-width
C	SDOF (HSS) stress strength conversion coefficient
C_{ij}	fitting coefficients associated with FP correlation curves
COD	coefficient of determination
C_u	importance coefficient
d	HSS dimension
DM_{dyn}	relevant peak dynamic DM response
DM_{lim}	relevant capacity DM response
f	frequency
f_a	SDOF elastic frequency
f_0, f_1, f_2	frequency constants associated with seismic demand formulation
g	gravity acceleration constant (unit)
h	RB semi-height
H	SDOF height
H_B	building height
h/b	RB slenderness
m	SDOF mass
N	SDOF (HSS) applied axial force
N_y	SDOF (HSS) yielding axial force
p	RB frequency parameter
PFA	peak floor acceleration
PGA	peak ground acceleration
PGA*	RB dimensionless peak ground acceleration
PGV	peak ground velocity
PGV*	RB dimensionless peak ground velocity
P_{VR}	target earthquake probability of exceedance within V_R
R	semi-diagonal block size
S	stratigraphic coefficient
Sa	(pseudo-)spectral acceleration
S_{ij}	fitting coefficients associated with FP correlation surfaces
t	HSS thickness
T_C	code spectral period
T_R	return period
T_r	RB rocking period
T_1	fundamental building period
$\ddot{u}_g$	RB time history base acceleration input
V_N	nominal life
x_M	FP median
$\overline{X}$	SDOF parameter

(*continued on next page*)

Table A1 (*continued*)

Abbreviations	
X,Y,Z	FP correlation surface dimensions
z	NE installation height (within the building)
α	RB critical angle
α_g	LS design PGA on stiff soil expressed in g unit
Δ	SDOF (HSS) lateral mass displacement Δ
θ	RB rotation angle
θ_0	initial (or release) RB rotation angle
θ_{max}	peak RB rotation angle
μ	SDOF (HSS) ductility capacity
σ	FP logarithmic standard deviation
σ_y	SDOF (HSS) yielding strength

Table A2
Constants (C_{1X}) and coefficient of determination (COD) associated with the fitting equations of rigid blocks (RBs) fragility median (x_M), considering dimensionless peak ground acceleration (PGA*), as a function of semi-diagonal block dimension (R), for investigated values of limit dimensionless rocking amplitude angle ($|\theta_{max}/\alpha|_{lim}$) and considering strong ground motion (SGM), floor motion (FM), and strong floor motion (SFM) sets; R is expressed in m.

$x_M\|PGA^* = C_{11}\bullet R^3 + C_{12}\bullet R^2 + C_{13}\bullet R + C_{14}$		$\|\theta_{max}/\alpha\|_{lim}$											
		0.01	0.05	0.1	0.2	0.3	0.4	0.5	0.6	0.7	0.8	0.9	1
SGM	C_{11}	0.002	0.001	0.000	0.000	0.003	0.000	−0.007	−0.009	−0.010	−0.012	−0.012	−0.011
	C_{12}	−0.014	−0.009	0.000	0.003	−0.011	0.014	0.059	0.074	0.080	0.083	0.082	0.077
	C_{13}	0.051	0.061	0.067	0.124	0.184	0.202	0.188	0.206	0.246	0.293	0.332	0.345
	C_{14}	1.184	1.200	1.213	1.214	1.217	1.219	1.241	1.243	1.236	1.222	1.209	1.209
	COD	**0.947**	**0.992**	**0.996**	**0.998**	**0.998**	**0.999**	**0.999**	**1.000**	**0.999**	**1.000**	**0.999**	**0.999**
FM	C_{11}	0.000	0.006	−0.008	−0.003	−0.001	0.011	0.003	0.024	0.044	0.017	0.000	−0.005
	C_{12}	0.002	−0.031	0.068	0.009	0.004	−0.081	−0.031	−0.130	−0.271	−0.084	0.032	0.066
	C_{13}	0.010	0.094	0.002	0.319	0.443	0.712	0.742	0.949	1.305	1.069	0.922	0.874
	C_{14}	0.519	0.506	0.554	0.444	0.457	0.421	0.439	0.396	0.290	0.388	0.464	0.490
	COD	**0.976**	**0.997**	**0.999**	**0.998**	**1.000**	**0.998**	**0.997**	**0.998**	**0.997**	**0.999**	**0.997**	**0.998**
SFM	C_{11}	−0.001	0.003	−0.006	−0.007	0.003	0.000	0.002	−0.014	0.000	0.002	0.002	−0.001
	C_{12}	0.002	−0.014	0.055	0.051	0.004	0.019	−0.013	0.098	−0.004	−0.026	−0.035	−0.016
	C_{13}	0.010	0.036	−0.051	0.086	0.201	0.278	0.458	0.279	0.538	0.661	0.697	0.686
	C_{14}	0.511	0.512	0.541	0.475	0.486	0.459	0.378	0.474	0.373	0.319	0.329	0.331
	COD	**0.701**	**0.994**	**0.997**	**0.996**	**0.995**	**0.990**	**0.999**	**0.999**	**0.997**	**0.996**	**0.994**	**0.993**

Table A3
Constants (C_{1X}) and coefficient of determination (COD) associated with the fitting equations of rigid blocks (RBs) fragility median (x_M), considering dimensionless peak ground acceleration (PGA*), as a function of block frequency parameter (p), for investigated values of limit dimensionless rocking amplitude angle ($|\theta_{max}/\alpha|_{lim}$) and considering strong ground motion (SGM), floor motion (FM), and strong floor motion (SFM) sets; p is expressed in Hz.

$x_M\|PGA^* = C_{11}\bullet p^3 + C_{12}\bullet p^2 + C_{13}\bullet p + C_{14}$		$\|\theta_{max}/\alpha\|_{lim}$											
		0.01	0.05	0.1	0.2	0.3	0.4	0.5	0.6	0.7	0.8	0.9	1
SGM	C_{11}	−0.003	−0.012	−0.032	−0.046	−0.099	−0.119	−0.125	−0.152	−0.162	−0.159	−0.151	−0.154
	C_{12}	0.033	0.128	0.324	0.481	0.998	1.214	1.299	1.567	1.687	1.674	1.612	1.642
	C_{13}	−0.127	−0.454	−1.088	−1.681	−3.290	−4.083	−4.468	−5.355	−5.810	−5.865	−5.754	−5.858
	C_{14}	1.385	1.782	2.477	3.262	4.924	5.910	6.506	7.500	8.100	8.316	8.336	8.458
	COD	**0.949**	**0.991**	**0.994**	**0.995**	**0.990**	**0.994**	**0.999**	**0.999**	**0.998**	**1.000**	**0.999**	**0.999**
FM	C_{11}	−0.004	−0.042	−0.073	−0.081	−0.157	−0.211	−0.228	−0.365	−0.394	−0.410	−0.421	−0.429
	C_{12}	0.039	0.412	0.753	0.900	1.647	2.165	2.382	3.706	4.012	4.222	4.359	4.440
	C_{13}	−0.140	−1.303	−2.537	−3.344	−5.752	−7.423	−8.341	−12.395	−13.484	−14.382	−14.928	−15.222
	C_{14}	0.698	1.898	3.402	4.818	7.482	9.404	10.726	14.734	16.108	17.362	18.114	18.464
	COD	**0.975**	**0.945**	**0.999**	**0.998**	**0.998**	**0.994**	**0.995**	**0.987**	**0.979**	**0.991**	**0.993**	**0.995**
SFM	C_{11}	0.001	−0.021	−0.039	−0.047	−0.141	−0.170	−0.148	−0.155	−0.155	−0.148	−0.148	−0.138
	C_{12}	−0.003	0.205	0.396	0.531	1.414	1.724	1.559	1.654	1.693	1.649	1.646	1.561
	C_{13}	−0.008	−0.643	−1.323	−1.989	−4.629	−5.745	−5.485	−5.874	−6.162	−6.172	−6.143	−5.930
	C_{14}	0.555	1.178	1.973	3.021	5.616	7.002	7.132	7.655	8.197	8.445	8.450	8.317
	COD	**0.659**	**0.906**	**0.998**	**0.997**	**0.987**	**0.986**	**0.996**	**0.998**	**0.994**	**0.995**	**0.993**	**0.993**

Table A4
Constants (C_{1X}) and coefficient of determination (COD) associated with the fitting equations of rigid blocks (RBs) fragility median (x_M), considering dimensionless peak ground velocity (PGV*), as a function of semi-diagonal block dimension (R), for investigated values of limit dimensionless rocking amplitude angle ($|\theta_{max}/\alpha|_{lim}$) and considering strong ground motion (SGM), floor motion (FM), and strong floor motion (SFM) sets; R is expressed in m.

$x_M\|PGV^* = C_{11}\bullet R^3 + C_{12}\bullet R^2 + C_{13}\bullet R + C_{14}$		$\|\theta_{max}/\alpha\|_{lim}$											
		0.01	0.05	0.1	0.2	0.3	0.4	0.5	0.6	0.7	0.8	0.9	1
SGM	C_{11}	−0.017	−0.018	−0.018	−0.018	−0.017	−0.017	−0.019	−0.019	−0.019	−0.018	−0.018	−0.018
	C_{12}	0.165	0.168	0.170	0.168	0.163	0.166	0.172	0.172	0.169	0.166	0.163	0.163
	C_{13}	−0.524	−0.528	−0.528	−0.515	−0.500	−0.493	−0.493	−0.482	−0.467	−0.450	−0.438	−0.438
	C_{14}	0.798	0.810	0.819	0.827	0.834	0.839	0.850	0.851	0.851	0.848	0.846	0.849
	COD	**0.992**	**0.991**	**0.991**	**0.988**	**0.991**	**0.986**	**0.986**	**0.987**	**0.984**	**0.979**	**0.967**	**0.964**
FM	C_{11}	−0.005	−0.004	−0.006	−0.004	−0.003	−0.001	−0.002	0.000	0.003	−0.001	−0.002	−0.003
	C_{12}	0.046	0.042	0.052	0.035	0.029	0.013	0.017	0.006	−0.014	0.007	0.020	0.025
	C_{13}	−0.142	−0.132	−0.141	−0.082	−0.061	−0.020	−0.016	0.006	0.054	0.026	0.010	0.001
	C_{14}	0.205	0.207	0.216	0.201	0.211	0.215	0.225	0.227	0.220	0.235	0.248	0.253
	COD	**0.986**	**0.983**	**0.978**	**0.692**	**0.946**	**0.972**	**0.970**	**0.986**	**0.973**	**0.987**	**0.982**	**0.988**
SFM	C_{11}	−0.006	−0.006	−0.007	−0.006	−0.005	−0.004	−0.003	−0.006	−0.004	−0.003	−0.003	−0.003
	C_{12}	0.055	0.054	0.063	0.055	0.045	0.040	0.028	0.049	0.033	0.024	0.020	0.021
	C_{13}	−0.168	−0.169	−0.179	−0.141	−0.121	−0.094	−0.054	−0.093	−0.054	−0.023	−0.014	−0.013
	C_{14}	0.243	0.248	0.251	0.235	0.245	0.237	0.222	0.247	0.235	0.223	0.227	0.227
	COD	**0.987**	**0.982**	**0.980**	**0.886**	**0.924**	**0.853**	**0.928**	**0.938**	**0.847**	**0.861**	**0.880**	**0.878**

Table A5
Constants (C_{1X}) and coefficient of determination (COD) associated with the fitting equations of rigid blocks (RBs) fragility median (x_M), considering dimensionless peak ground velocity (PGV*), as a function of block frequency parameter (p), for investigated values of limit dimensionless rocking amplitude angle ($|\theta_{max}/\alpha|_{lim}$) and considering strong ground motion (SGM), floor motion (FM), and strong floor motion (SFM) sets; p is expressed in Hz.

$x_M\|PGV^* = C_{11}\bullet p^3 + C_{12}\bullet p^2 + C_{13}\bullet p + C_{14}$		$\|\theta_{max}/\alpha\|_{lim}$											
		0.01	0.05	0.1	0.2	0.3	0.4	0.5	0.6	0.7	0.8	0.9	1
SGM	C_{11}	−0.003	−0.004	−0.006	−0.006	−0.014	−0.014	−0.013	−0.016	−0.016	−0.014	−0.010	−0.010
	C_{12}	0.021	0.028	0.053	0.053	0.129	0.135	0.132	0.163	0.166	0.144	0.116	0.116
	C_{13}	0.106	0.078	−0.001	−0.021	−0.250	−0.297	−0.307	−0.412	−0.434	−0.385	−0.317	−0.319
	C_{14}	0.034	0.077	0.169	0.234	0.475	0.570	0.624	0.754	0.808	0.796	0.759	0.767
	COD	**1.000**	**1.000**	**1.000**	**1.000**	**0.999**	**0.999**	**0.999**	**0.999**	**0.998**	**0.998**	**0.994**	**0.996**
FM	C_{11}	0.000	−0.003	−0.004	0.000	−0.006	−0.010	−0.009	−0.019	−0.018	−0.018	−0.019	−0.019
	C_{12}	0.002	0.030	0.046	0.008	0.067	0.105	0.095	0.198	0.189	0.194	0.205	0.209
	C_{13}	0.029	−0.056	−0.125	−0.050	−0.230	−0.337	−0.336	−0.653	−0.643	−0.687	−0.730	−0.747
	C14	0.010	0.101	0.206	0.215	0.422	0.554	0.608	0.931	0.966	1.053	1.117	1.143
	COD	**1.000**	**0.996**	**0.998**	**0.975**	**0.986**	**0.966**	**0.974**	**0.967**	**0.932**	**0.983**	**0.983**	**0.990**
SFM	C_{11}	0.000	−0.002	−0.003	0.001	−0.011	−0.013	−0.005	−0.005	0.000	0.003	0.002	0.004
	C_{12}	0.000	0.018	0.031	0.004	0.113	0.126	0.064	0.070	0.025	−0.002	0.007	−0.007
	C_{13}	0.045	−0.012	−0.066	−0.023	−0.328	−0.386	−0.236	−0.268	−0.168	−0.104	−0.118	−0.084
	C_{14}	0.000	0.058	0.132	0.155	0.447	0.547	0.465	0.516	0.471	0.447	0.457	0.434
	COD	**1.000**	**0.998**	**0.999**	**0.995**	**0.927**	**0.854**	**0.985**	**0.978**	**0.967**	**0.969**	**0.956**	**0.954**

Table A6
Constants (C_{1X}) and coefficient of determination (COD) associated with the fitting equations of rigid blocks (RBs) fragility logarithmic standard deviation (σ), considering dimensionless peak ground acceleration (PGA*), as a function of semi-diagonal block dimension (R), for investigated values of limit dimensionless rocking amplitude angle ($|\theta_{max}/\alpha|_{lim}$) and considering strong ground motion (SGM), floor motion (FM), and strong floor motion (SFM) sets; R is expressed in m.

$\sigma\|PGA^* = C_{11}\bullet R^3 + C_{12}\bullet R^2 + C_{13}\bullet R + C_{14}$		$\|\theta_{max}/\alpha\|_{lim}$											
		0.01	0.05	0.1	0.2	0.3	0.4	0.5	0.6	0.7	0.8	0.9	1
SGM	C_{11}	0.002	0.001	0.000	0.000	0.003	0.000	−0.007	−0.009	−0.010	−0.012	−0.012	−0.011
	C_{12}	−0.014	−0.009	0.000	0.003	−0.011	0.014	0.059	0.074	0.080	0.083	0.082	0.077
	C_{13}	0.051	0.061	0.067	0.124	0.184	0.202	0.188	0.206	0.246	0.293	0.332	0.345
	C_{14}	1.184	1.200	1.213	1.214	1.217	1.219	1.241	1.243	1.236	1.222	1.209	1.209
	COD	**0.947**	**0.992**	**0.996**	**0.998**	**0.998**	**0.999**	**0.999**	**1.000**	**0.999**	**1.000**	**0.999**	**0.999**
FM	C_{11}	0.000	0.006	−0.008	−0.003	−0.001	0.011	0.003	0.024	0.044	0.017	0.000	−0.005
	C_{12}	0.002	−0.031	0.068	0.009	0.004	−0.081	−0.031	−0.130	−0.271	−0.084	0.032	0.066
	C_{13}	0.010	0.094	0.002	0.319	0.443	0.712	0.742	0.949	1.305	1.069	0.922	0.874
	C_{14}	0.519	0.506	0.554	0.444	0.457	0.421	0.439	0.396	0.290	0.388	0.464	0.490
	COD	**0.976**	**0.997**	**0.999**	**0.998**	**1.000**	**0.998**	**0.997**	**0.998**	**0.997**	**0.999**	**0.997**	**0.998**
SFM	C_{11}	−0.001	0.003	−0.006	−0.007	0.003	0.000	0.002	−0.014	0.000	0.002	0.002	−0.001
	C_{12}	0.002	−0.014	0.055	0.051	0.004	0.019	−0.013	0.098	−0.004	−0.026	−0.035	−0.016
	C_{13}	0.010	0.036	−0.051	0.086	0.201	0.278	0.458	0.279	0.538	0.661	0.697	0.686
	C_{14}	0.511	0.512	0.541	0.475	0.486	0.459	0.378	0.474	0.373	0.319	0.329	0.331
	COD	**0.701**	**0.994**	**0.997**	**0.996**	**0.995**	**0.990**	**0.999**	**0.999**	**0.997**	**0.996**	**0.994**	**0.993**

Table A7
Constants (C_{1X}) and coefficient of determination (COD) associated with the fitting equations of rigid blocks (RBs) fragility logarithmic standard deviation (σ), considering dimensionless peak ground acceleration (PGA*), as a function of block frequency parameter (p), for investigated values of limit dimensionless rocking amplitude angle ($|\theta_{max}/\alpha|_{lim}$) and considering strong ground motion (SGM), floor motion (FM), and strong floor motion (SFM) sets; p is expressed in Hz.

$\sigma\|PGA^* = C_{11}\bullet p^3 + C_{12}\bullet p^2 + C_{13}\bullet p + C_{14}$		$\|\theta_{max}/\alpha\|_{lim}$											
		0.01	0.05	0.1	0.2	0.3	0.4	0.5	0.6	0.7	0.8	0.9	1
SGM	C_{11}	−0.003	−0.012	−0.032	−0.046	−0.099	−0.119	−0.125	−0.152	−0.162	−0.159	−0.151	−0.154
	C_{12}	0.033	0.128	0.324	0.481	0.998	1.214	1.299	1.567	1.687	1.674	1.612	1.642
	C_{13}	−0.127	−0.454	−1.088	−1.681	−3.290	−4.083	−4.468	−5.355	−5.810	−5.865	−5.754	−5.858
	C_{14}	1.385	1.782	2.477	3.262	4.924	5.910	6.506	7.500	8.100	8.316	8.336	8.458
	COD	**0.949**	**0.991**	**0.994**	**0.995**	**0.990**	**0.994**	**0.999**	**0.999**	**0.998**	**1.000**	**0.999**	**0.999**
FM	C_{11}	−0.004	−0.042	−0.073	−0.081	−0.157	−0.211	−0.228	−0.365	−0.394	−0.410	−0.421	−0.429
	C_{12}	0.039	0.412	0.753	0.900	1.647	2.165	2.382	3.706	4.012	4.222	4.359	4.440
	C_{13}	−0.140	−1.303	−2.537	−3.344	−5.752	−7.423	−8.341	−12.395	−13.484	−14.382	−14.928	−15.222
	C_{14}	0.698	1.898	3.402	4.818	7.482	9.404	10.726	14.734	16.108	17.362	18.114	18.464
	COD	**0.975**	**0.945**	**0.999**	**0.998**	**0.998**	**0.994**	**0.995**	**0.987**	**0.979**	**0.991**	**0.993**	**0.995**
SFM	C_{11}	0.001	−0.021	−0.039	−0.047	−0.141	−0.170	−0.148	−0.155	−0.155	−0.148	−0.148	−0.138
	C_{12}	−0.003	0.205	0.396	0.531	1.414	1.724	1.559	1.654	1.693	1.649	1.646	1.561
	C_{13}	−0.008	−0.643	−1.323	−1.989	−4.629	−5.745	−5.485	−5.874	−6.162	−6.172	−6.143	−5.930
	C_{14}	0.555	1.178	1.973	3.021	5.616	7.002	7.132	7.655	8.197	8.445	8.450	8.317
	COD	**0.659**	**0.906**	**0.998**	**0.997**	**0.987**	**0.986**	**0.996**	**0.998**	**0.994**	**0.995**	**0.993**	**0.993**

Table A8
Constants (C_{1X}) and coefficient of determination (COD) associated with the fitting equations of rigid blocks (RBs) fragility logarithmic standard deviation (σ), considering dimensionless peak ground velocity (PGV*), as a function of semi-diagonal block dimension (R), for investigated values of limit dimensionless rocking amplitude angle ($|\theta_{max}/\alpha|_{lim}$) and considering strong ground motion (SGM), floor motion (FM), and strong floor motion (SFM) sets; R is expressed in m.

$\sigma\|PGV^* = C_{11}\bullet R^3 + C_{12}\bullet R^2 + C_{13}\bullet R + C_{14}$		$\|\theta_{max}/\alpha\|_{lim}$											
		0.01	0.05	0.1	0.2	0.3	0.4	0.5	0.6	0.7	0.8	0.9	1
SGM	C_{11}	−0.017	−0.018	−0.018	−0.018	−0.017	−0.017	−0.019	−0.019	−0.019	−0.018	−0.018	−0.018
	C_{12}	0.165	0.168	0.170	0.168	0.163	0.166	0.172	0.172	0.169	0.166	0.163	0.163
	C_{13}	−0.524	−0.528	−0.528	−0.515	−0.500	−0.493	−0.493	−0.482	−0.467	−0.450	−0.438	−0.438
	C_{14}	0.798	0.810	0.819	0.827	0.834	0.839	0.850	0.851	0.851	0.848	0.846	0.849
	COD	**0.992**	**0.991**	**0.991**	**0.988**	**0.991**	**0.986**	**0.986**	**0.987**	**0.984**	**0.979**	**0.967**	**0.964**
FM	C_{11}	−0.005	−0.004	−0.006	−0.004	−0.003	−0.001	−0.002	0.000	0.003	−0.001	−0.002	−0.003
	C_{12}	0.046	0.042	0.052	0.035	0.029	0.013	0.017	0.006	−0.014	0.007	0.020	0.025
	C_{13}	−0.142	−0.132	−0.141	−0.082	−0.061	−0.020	−0.016	0.006	0.054	0.026	0.010	0.001
	C_{14}	0.205	0.207	0.216	0.201	0.211	0.215	0.225	0.227	0.220	0.235	0.248	0.253
	COD	**0.986**	**0.983**	**0.978**	**0.692**	**0.946**	**0.972**	**0.970**	**0.986**	**0.973**	**0.987**	**0.982**	**0.988**
SFM	C_{11}	−0.006	−0.006	−0.007	−0.006	−0.005	−0.004	−0.003	−0.006	−0.004	−0.003	−0.003	−0.003
	C_{12}	0.055	0.054	0.063	0.055	0.045	0.040	0.028	0.049	0.033	0.024	0.020	0.021
	C_{13}	−0.168	−0.169	−0.179	−0.141	−0.121	−0.094	−0.054	−0.093	−0.054	−0.023	−0.014	−0.013
	C_{14}	0.243	0.248	0.251	0.235	0.245	0.237	0.222	0.247	0.235	0.223	0.227	0.227
	COD	**0.987**	**0.982**	**0.980**	**0.886**	**0.924**	**0.853**	**0.928**	**0.938**	**0.847**	**0.861**	**0.880**	**0.878**

Table A9
Constants (C_{1X}) and coefficient of determination (COD) associated with the fitting equations of rigid blocks (RBs) fragility logarithmic standard deviation (σ), considering dimensionless peak ground velocity (PGV*), as a function of block frequency parameter (p), for investigated values of limit dimensionless rocking amplitude angle ($|\theta_{max}/\alpha|_{lim}$) and considering strong ground motion (SGM), floor motion (FM), and strong floor motion (SFM) sets; p is expressed in Hz.

$\sigma\|PGV^* = C_{11}\bullet p^3 + C_{12}\bullet p^2 + C_{13}\bullet p + C_{14}$		$\|\theta_{max}/\alpha\|_{lim}$											
		0.01	0.05	0.1	0.2	0.3	0.4	0.5	0.6	0.7	0.8	0.9	1
SGM	C_{11}	−0.003	−0.004	−0.006	−0.006	−0.014	−0.014	−0.013	−0.016	−0.016	−0.014	−0.010	−0.010
	C_{12}	0.021	0.028	0.053	0.053	0.129	0.135	0.132	0.163	0.166	0.144	0.116	0.116
	C_{13}	0.106	0.078	−0.001	−0.021	−0.250	−0.297	−0.307	−0.412	−0.434	−0.385	−0.317	−0.319
	C_{14}	0.034	0.077	0.169	0.234	0.475	0.570	0.624	0.754	0.808	0.796	0.759	0.767
	COD	**1.000**	**1.000**	**1.000**	**1.000**	**0.999**	**0.999**	**0.999**	**0.999**	**0.998**	**0.998**	**0.994**	**0.996**
FM	C_{11}	0.000	−0.003	−0.004	0.000	−0.006	−0.010	−0.009	−0.019	−0.018	−0.018	−0.019	−0.019
	C_{12}	0.002	0.030	0.046	0.008	0.067	0.105	0.095	0.198	0.189	0.194	0.205	0.209
	C_{13}	0.029	−0.056	−0.125	−0.050	−0.230	−0.337	−0.336	−0.653	−0.643	−0.687	−0.730	−0.747
	C_{14}	0.010	0.101	0.206	0.215	0.422	0.554	0.608	0.931	0.966	1.053	1.117	1.143
	COD	**1.000**	**0.996**	**0.998**	**0.975**	**0.986**	**0.966**	**0.974**	**0.967**	**0.932**	**0.983**	**0.983**	**0.990**
SFM	C_{11}	0.000	−0.002	−0.003	0.001	−0.011	−0.013	−0.005	−0.005	0.000	0.003	0.002	0.004
	C_{12}	0.000	0.018	0.031	0.004	0.113	0.126	0.064	0.070	0.025	−0.002	0.007	−0.007
	C_{13}	0.045	−0.012	−0.066	−0.023	−0.328	−0.386	−0.236	−0.268	−0.168	−0.104	−0.118	−0.084
	C_{14}	0.000	0.058	0.132	0.155	0.447	0.547	0.465	0.516	0.471	0.447	0.457	0.434
	COD	**1.000**	**0.998**	**0.999**	**0.995**	**0.927**	**0.854**	**0.985**	**0.978**	**0.967**	**0.969**	**0.956**	**0.954**

Table A10
Constants (S_{XY}) and coefficient of determination (COD) associated with the fitting equations of rigid blocks (RBs) fragility median (x_M), considering dimensionless peak ground acceleration (PGA*) and velocity (PGV*), as a function of semi-diagonal block dimension (R) or block frequency parameter (p) and limit dimensionless rocking amplitude angle ($|\theta_{max}/\alpha|_{lim}$), and considering strong ground motion (SGM), floor motion (FM), and strong floor motion (SFM) sets; R is expressed in m; p is expressed in Hz.

$x_M\|Z = (x,y) = S_{00} + S_{10}\bullet X + S_{01}\bullet Y + S_{20}\bullet X^2 + S_{11}\bullet X\bullet Y + S_{02}\bullet Y^2$		$X = \|\theta_{max}/\alpha\|_{lim}$			
		Z = PGA*		Z = PGV*	
		Y = R	Y = p	Y = R	Y = p
SGM	S_{00}	1.143	2.406	0.649	0.090
	S_{10}	0.459	2.963	0.191	0.539
	S_{01}	0.032	−0.948	−0.232	0.079
	S_{20}	−0.543	−0.543	−0.123	−0.123
	S_{11}	0.505	−0.621	0.067	−0.088
	S_{02}	0.001	0.163	0.030	0.012
	COD	**0.992**	**0.937**	**0.923**	**0.987**
FM	S_{00}	0.424	3.025	0.139	0.141
	S_{10}	0.973	6.551	0.245	0.677
	S_{01}	−0.022	−2.029	−0.420	−0.079
	S_{20}	−1.160	−1.160	−0.153	−0.153
	S_{11}	1.135	−1.376	0.085	−0.109
	S_{02}	0.018	0.350	0.005	0.020
	COD	**0.993**	**0.928**	**0.986**	**0.966**
SFM	S_{00}	0.373	1.986	0.165	0.111
	S_{10}	0.633	3.793	0.153	0.474
	S_{01}	0.054	−1.202	−0.485	−0.048
	S_{20}	−0.765	−0.765	−0.107	−0.107
	S_{11}	0.631	−0.789	0.061	−0.083
	S_{02}	−0.001	0.206	0.005	0.016
	COD	**0.984**	**0.937**	**0.935**	**0.957**

Table A11
Constants (C_{1X}) and coefficient of determination (COD) associated with the fitting equations of single-degree-of-freedom (SDOF) systems fragility median (x_M), considering peak ground acceleration (PGA), as a function of SDOF frequency (f_a), for investigated damage states (DSs), and considering floor motion (FM) and strong floor motion (SFM) sets; f is expressed in Hz; PGA is expressed in g.

$x_M\|PGA = C_{11}\bullet f_a + C_{12}$		DS				
		DS1	DS2	DS3	DS4	DS5
FM	C_{11}	0.076	0.148	0.225	0.230	0.168
	C_{12}	0.119	0.254	0.433	0.904	1.705
	COD	**0.803**	**0.795**	**0.832**	**0.737**	**0.511**
SFM	C_{11}	0.080	0.156	0.231	0.230	0.170
	C_{12}	0.079	0.172	0.294	0.672	1.365
	COD	**0.767**	**0.757**	**0.823**	**0.794**	**0.585**

Table A12
Constants (C_{1X}) and coefficient of determination (COD) associated with the fitting equations of single-degree-of-freedom (SDOF) systems fragility median (x_M), considering peak ground acceleration (PGA), as a function of SDOF frequency (f_a), for investigated damage states (DSs), and considering floor motion (FM) and strong floor motion (SFM) sets; f is expressed in Hz; PGV is expressed in m/s.

$x_M\|PGV = C_{11}\bullet f_a + C_{12}$		DS				
		DS1	DS2	DS3	DS4	DS5
FM	C_{11}	0.006	0.012	0.018	0.019	0.014
	C_{12}	0.01	0.021	0.035	0.074	0.139
	COD	**0.803**	**0.795**	**0.832**	**0.737**	**0.511**
SFM	C_{11}	0.007	0.013	0.02	0.02	0.015
	C_{12}	0.007	0.015	0.025	0.058	0.117
	COD	**0.767**	**0.757**	**0.823**	**0.794**	**0.585**

Table A13
Constants (C_{1X}) and coefficient of determination (COD) associated with the fitting equations of single-degree-of-freedom (SDOF) systems fragility logarithmic standard deviation (σ), considering peak ground acceleration (PGA), as a function of SDOF frequency (f_a), for investigated damage states (DSs), and considering floor motion (FM) and strong floor motion (SFM) sets; f is expressed in Hz; PGA is expressed in g.

$\sigma\|PGA = C_{11}\bullet f_a^2 + C_{12}\bullet f_a + C_{13}$		DS				
		DS1	DS2	DS3	DS4	DS5
FM	C_{11}	0.011	0.009	0.012	0.015	0.013
	C_{12}	−0.175	−0.156	−0.186	−0.222	−0.201
	C_{13}	1.119	1.071	1.07	1.144	1.162
	COD	**0.969**	**0.979**	**0.989**	**0.968**	**0.984**
SFM	C_{11}	−0.027	−0.028	−0.021	−0.009	0.005
	C_{12}	0.278	0.291	0.223	0.116	−0.031
	C_{13}	0.068	0.037	0.069	0.106	0.358
	COD	**0.64**	**0.656**	**0.72**	**0.886**	**0.346**

Table A14
Constants (C_{1X}) and coefficient of determination (COD) associated with the fitting equations of single-degree-of-freedom (SDOF) systems logarithmic standard deviation (σ), considering peak ground acceleration (PGA), as a function of SDOF frequency (f_a), for investigated damage states (DSs), and considering floor motion (FM) and strong floor motion (SFM) sets; f is expressed in Hz; PGV is expressed in m/s.

$\sigma\|PGV = C_{11}\bullet f_a^2 + C_{12}\bullet f_a + C_{13}$		DS				
		DS1	DS2	DS3	DS4	DS5
FM	C_{11}	−0.005	−0.006	0.002	0.008	0.009
	C_{12}	0.058	0.065	−0.019	−0.095	−0.116
	C_{13}	0.59	0.565	0.647	0.741	0.785
	COD	**0.408**	**0.618**	**0.152**	**0.675**	**0.922**
SFM	C_{11}	−0.019	−0.019	−0.015	−0.009	−0.008
	C_{12}	0.198	0.197	0.159	0.105	0.108
	C_{13}	0.364	0.358	0.358	0.377	0.294
	COD	**0.767**	**0.792**	**0.745**	**0.651**	**0.759**

Table A15
Constants (S_{XY}) and coefficient of determination (COD) associated with the fitting equations of single-degree-of-freedom (SDOF) systems fragility median (x_M), considering peak ground acceleration (PGA) and velocity (PGV), as a function of SDOF frequency (f_a) and limit dimensionless displacement ($|\Delta_{max}|_{lim}/|\Delta_{max}|_{DS5}$), considering floor motion (FM) and strong floor motion (SFM) sets; f_a is expressed in Hz; PGA is expressed in g; PGV is expressed in m/s.

$x_M\|Z = (x,y) = S_{00} + S_{10}\bullet X + S_{01}\bullet Y + S_{11}\bullet X\bullet Y + S_{02}\bullet Y^2$		$X = f_a$	
		$Y = \|\Delta_{max}\|_{lim}/\|\Delta_{max}\|_{DS5}$	
		Z = PGA	Z = PGV
FM	S_{00}	−0.667	−0.054
	S_{10}	0.233	0.019
	S_{01}	4.963	0.404
	S_{11}	−0.030	−0.002
	S_{02}	−2.717	−0.221
	COD	**0.836**	**0.836**
SFM	S_{00}	−0.626	−0.054
	S_{10}	0.228	0.020
	S_{01}	4.239	0.363
	S_{11}	−0.029	−0.002
	S_{02}	−2.356	−0.202
	COD	**0.825**	**0.825**

Data availability

Data will be made available on request.

References

[1] Liu J, Zhai C, Yu P. A probabilistic framework to evaluate seismic resilience of hospital buildings using Bayesian networks. Reliab Eng Syst Saf 2022;226:108644. https://doi.org/10.1016/j.ress.2022.108644.

[2] Ceferino L, Mitrani-Reiser J, Kiremidjian A, Deierlein G, Bambarén C. Effective plans for hospital system response to earthquake emergencies. Nat Commun 2020;11:4325. https://doi.org/10.1038/s41467-020-18072-w.

[3] Quinci G, Paolacci F, Fragiadakis M, Bursi OS. A machine learning framework for seismic risk assessment of industrial equipment. Reliab Eng Syst Saf 2025;254:110606. https://doi.org/10.1016/j.ress.2024.110606.

[4] Ghith A, Ezzeldin M, Tait M, El-Dakhakhni W. Shake table seismic performance assessment of auxiliary battery power systems using the FEMA 461 protocol. J Struct Eng 2019;145:04019080. https://doi.org/10.1061/(ASCE)ST.1943-541X.0002341.

[5] Butenweg C, Bursi OS, Paolacci F, Marinković M, Lanese I, Nardin C, Quinci G. Seismic performance of an industrial multi-storey frame structure with process

equipment subjected to shake table testing. Eng Struct 2021;243:112681. https://doi.org/10.1016/j.engstruct.2021.112681.
[6] Perrone D, Brunesi E, Filiatrault A, Peloso S, Nascimbene R, Beiter C, Piccinin R. Seismic numerical modelling of suspended piping trapeze restraint installations based on component testing. Bull Earthq Eng 2020;18:3247–83. https://doi.org/10.1007/s10518-020-00832-0.
[7] Feinstein T, Moehle JP. Mechanics based numerical modeling of floor-anchored nonstructural components. J Struct Eng 2023;149:04022213. https://doi.org/10.1061/(ASCE)ST.1943-541X.0003496.
[8] British Standards Institution, European Committee for Standardization, Eurocode 8. Design of structures for earthquake resistance. London: British Standards Institution; 2005.
[9] American Society of Civil Engineers. Minimum design loads and associated criteria for buildings and other structures. 7th ed. Reston, VA: American Society of Civil Engineers; 2021. https://doi.org/10.1061/9780784415788.
[10] Ministero delle Infrastrutture e dei Trasporti, D.M. del 17/01/2018—"Aggiornamento delle Norme tecniche per le Costruzioni 2018" NTC 2018 (in Italian), (2018).
[11] Vukobratović V, Fajfar P. A method for the direct estimation of floor acceleration spectra for elastic and inelastic MDOF structures. Earthq Eng Struct Dyn 2016;45:2495–511. https://doi.org/10.1002/eqe.2779.
[12] Merino RJ, Perrone D, Filiatrault A. Consistent floor response spectra for performance-based seismic design of nonstructural elements. Earthq Eng Struct Dyn 2020;49:261–84. https://doi.org/10.1002/eqe.3236.
[13] Petrone C, Magliulo G, Manfredi G. Seismic demand on light acceleration-sensitive nonstructural components in European reinforced concrete buildings. Earthq Eng Struct Dyn 2015;44:1203–17. https://doi.org/10.1002/eqe.2508.
[14] Karalar M, Çavuşlu M, Mert N. Determination of 3D seismic performance of nonstructural elements in a collapsed RC building considering TBEC-2018. Teh Vjesn 2022;29. https://doi.org/10.17559/TV-20210112150414.
[15] Gesualdo A, Iannuzzo A, Minutolo V, Monaco M. Rocking of freestanding objects: theoretical and experimental comparisons. J Theor Appl Mech 2018;56:977–91. https://doi.org/10.15632/jtam-pl.56.4.977.
[16] Shenton III HW. Criteria for initiation of slide, rock, and slide-rock rigid-body modes. J Eng Mech 1996;122:690–3. https://doi.org/10.1061/(ASCE)0733-9399(1996)122:7(690).
[17] Aslam M, Scalise DT, Godden WG. Earthquake rocking response of rigid blocks. J Struct Eng Div (ASCE) 1980;106:377–92.
[18] Zhang J, Makris N. Rocking response of free-standing blocks under cycloidal pulses. J Eng Mech 2001;127:473–83. https://doi.org/10.1061/(ASCE)0733-9399(2001)127:5(473).
[19] Pürgstaller A, Gallo PQ, Pampanin S, Bergmeister K. Seismic demands on nonstructural components anchored to concrete accounting for structure-fastener-nonstructural interaction (SFNI). Earthq Eng Struct Dyn 2020;49:589–606. https://doi.org/10.1002/eqe.3255.
[20] Feinstein T, Moehle JP. Seismic response of floor-anchored nonstructural components fastened with yielding elements. Earthq Eng Struct Dyn 2022;51:3–21. https://doi.org/10.1002/eqe.3553.
[21] Milne J. Seismic experiments. Trans Seismol Soc Jpn 1885;8:1–82.
[22] Kirkpatrick P. Seismic measurements by the overthrow of columns. Bull Seismol Soc Am 1927;17:95–109. https://doi.org/10.1785/BSSA0170020095.
[23] Muto K, Umemure H, Sonobe Y. Study of the overturning vibration of slender structures. In: Proceedings of the second world conference on earthquake engineering; 1960. p. 1239–61.
[24] Housner GW. The behavior of inverted pendulum structures during earthquakes. Bull Seismol Soc Am 1963;53:403–17.
[25] Priestley MJN, Evison RJ, Carr AJ. Seismic response of structures free to rock on their foundations. Bull N Z Nat Soc Earthq Eng 1978;11:141–50.
[26] Yim C-S, Chopra AK, Penzien J. Rocking response of rigid blocks to earthquakes. Earthq Eng Struct Dyn 1980;8:565–87. https://doi.org/10.1002/eqe.4290080606.
[27] Purvance MD, Anooshehpoor A, Brune JN. Freestanding block overturning fragilities: numerical simulation and experimental validation. Earthq Eng Struct Dyn 2008;37:791–808. https://doi.org/10.1002/eqe.789.
[28] Makris N, Kampas G. Size versus slenderness: two competing parameters in the seismic stability of free-standing rocking columns. Bull Seismol Soc Am 2016;106:104–22. https://doi.org/10.1785/0120150138.
[29] Makris N, Vassiliou MF. Planar rocking response and stability analysis of an array of free-standing columns capped with a freely supported rigid beam. Earthq Eng Struct Dyn 2013;42:431–49. https://doi.org/10.1002/eqe.2222.
[30] Gesualdo A, Iannuzzo A, Monaco M, Penta F. Rocking of a rigid block freestanding on a flat pedestal. J Zhejiang Univ Sci A 2018;19:331–45. https://doi.org/10.1631/jzus.A1700061.
[31] Wittich CE, Hutchinson TC. Shake table tests of stiff, unattached, asymmetric structures. Earthq Eng Struct Dyn 2015;44:2425–43. https://doi.org/10.1002/eqe.2589.
[32] Makris N. A half-century of rocking isolation. Earthq Struct 2014;7:1187–221. https://doi.org/10.12989/EAS.2014.7.6.1187.
[33] Di Egidio A, Contento A, de Leo AM, Gardoni P. Dynamic and seismic protection of rigid-block-like elements and structures on deformable ground with mass-damper dynamic absorbers. J Eng Mech 2020;146:04020046. https://doi.org/10.1061/(ASCE)EM.1943-7889.0001782.
[34] Pellecchia D, Lo Feudo S, Vaiana N, Dion J, Rosati L. A procedure to model and design elastomeric-based isolation systems for the seismic protection of rocking art objects. Comput Aided Civ Eng 2021:mice.12775. https://doi.org/10.1111/mice.12775.
[35] Contento A, Di Egidio A. Investigations into the benefits of base isolation for non-symmetric rigid blocks. Earthq Eng Struct Dyn 2009;38:849–66. https://doi.org/10.1002/eqe.870.
[36] Konstantinidis D, Makris N. Experimental and analytical studies on the response of freestanding laboratory equipment to earthquake shaking. Earthq Eng Struct Dyn 2009;38:827–48. https://doi.org/10.1002/eqe.871.
[37] Dimitrakopoulos EG, Paraskeva TS. Dimensionless fragility curves for rocking response to near-fault excitations. Earthq Eng Struct Dyn 2015;44:2015–33. https://doi.org/10.1002/eqe.2571.
[38] D'Angela D, Magliulo G, Cosenza E. Seismic damage assessment of unanchored nonstructural components taking into account the building response. Struct Saf 2021;93:102126. https://doi.org/10.1016/j.strusafe.2021.102126.
[39] Fragiadakis M, Diamantopoulos S. Fragility and risk assessment of freestanding building contents. Earthq Eng Struct Dyn 2020;49:1028–48. https://doi.org/10.1002/eqe.3276.
[40] Petrone C, Di Sarno L, Magliulo G, Cosenza E. Numerical modelling and fragility assessment of typical freestanding building contents. Bull Earthq Eng 2017;15:1609–33. https://doi.org/10.1007/s10518-016-0034-1.
[41] Kazantzi AK, Lachanas CG, Vamvatsikos D. Seismic response distribution expressions for rocking building contents under ordinary ground motions. Bull Earthq Eng 2022;20:6659–82. https://doi.org/10.1007/s10518-022-01424-w.
[42] Anajafi H, Medina RA, Santini-Bell E. Inelastic floor spectra for designing anchored acceleration-sensitive nonstructural components. Bull Earthquake Eng 2020;18:2115–47. https://doi.org/10.1007/s10518-019-00760-8.
[43] Tamura I, Matsuura S, Shimazu R. yield strength reduction factor of nonlinear SDOF systems on the supporting structures. Seismic engineering, 8. Vancouver, British Columbia, Canada: American Society of Mechanical Engineers; 2016. https://doi.org/10.1115/PVP2016-63944. V008T08A029.
[44] Obando JC, Lopez-Garcia D. Inelastic displacement ratios for nonstructural components subjected to floor accelerations. J Earthq Eng 2018;22:569–94. https://doi.org/10.1080/13632469.2016.1244131.
[45] Kazantzi AK, Miranda E, Vamvatsikos D. Strength-reduction factors for the design of light nonstructural elements in buildings. Earthq Eng Struct Dyn 2020;49:1329–43. https://doi.org/10.1002/eqe.3292.
[46] Elkady A, Vamvatsikos D, Lignos D, Kazantzi AK, Miranda E. Experimental study to validate an improved approach to design acceleration-sensitive nonstructural components. In: Proceedings of the fifth international workshop on the seismic performance of non-structural elements (SPONSE), ATC-SPONSE; 2022. p. 202–13.
[47] Kazantzi AK, Karaferis ND, Melissianos VE, Vamvatsikos D. Acceleration-sensitive ancillary elements in industrial facilities: alternative seismic design approaches in the new Eurocode. Bull Earthq Eng 2023. https://doi.org/10.1007/s10518-023-01656-4.
[48] CEN, draft of new EN 1998–3. Eurocode 8: Design of structures for earthquake resistance—Part 4: Silos, tanks and pipelines, towers, masts and chimneys, (2022).
[49] Vukobratović V, Fajfar P. Direct floor response spectra for nonlinear nonstructural components. Bull Earthq Eng 2023. https://doi.org/10.1007/s10518-023-01818-4.
[50] Perrone D, Calvi PM, Nascimbene R, Fischer EC, Magliulo G. Seismic performance of non-structural elements during the 2016 Central Italy earthquake. Bull Earthq Eng 2019;17:5655–77. https://doi.org/10.1007/s10518-018-0361-5.
[51] Filiatrault A, Perrone D, Merino RJ, Calvi GM. Performance-based seismic design of nonstructural building elements. J Earthq Eng 2021;25:237–69. https://doi.org/10.1080/13632469.2018.1512910.
[52] Perrone D, Rodriguez D, Filiatrault A, Brunesi E, Beiter C, Piccinin R. A framework for the quantification of non-structural seismic performance factors. J Earthq Eng 2022;26:8468–94. https://doi.org/10.1080/13632469.2021.1991516.
[53] Liu P, Xue W, Pang H, Zhang Y-M, Chen H-T, Yang W-G. Seismic overturning fragility analysis for freestanding building contents subjected to horizontal bidirectional floor motions. Soil Dyn Earthq Eng 2022;161:107414. https://doi.org/10.1016/j.soildyn.2022.107414.
[54] Magliulo G, D'Angela D. Seismic response and capacity of inelastic acceleration-sensitive nonstructural elements subjected to building floor motions. Earthq Eng Struct Dyn 2024:eqe.4080. https://doi.org/10.1002/eqe.4080.
[55] Salari N, Konstantinidis D, Mohsenzadeh V, Wiebe L. Demands on acceleration-sensitive nonstructural components in special concentrically braced frame and special moment frame buildings. Eng Struct 2022;260:114031. https://doi.org/10.1016/j.engstruct.2022.114031.
[56] Filiatrault A, Sullivan T. Performance-based seismic design of nonstructural building components: the next frontier of earthquake engineering. Earthq Eng Eng Vib 2014;13:17–46. https://doi.org/10.1007/s11803-014-0238-9.
[57] Brandolese S, Fiorin L, Scotta R. Seismic demand and capacity assessment of suspended ceiling systems. Eng Struct 2019;193:219–37. https://doi.org/10.1016/j.engstruct.2019.05.034.
[58] D'Angela D, Magliulo G, Di Salvatore C, Zito M. Seismic assessment and qualification of acceleration-sensitive nonstructural elements through shake table testing: reliability of testing protocols and reliability-targeted safety factors. Eng Struct 2024. https://doi.org/10.1016/j.engstruct.2023.117271.
[59] D'Angela D, Magliulo G, Cosenza E. Towards a reliable seismic assessment of rocking components. Eng Struct 2021;230:111673. https://doi.org/10.1016/j.engstruct.2020.111673.
[60] D'Angela A, Magliulo G, Cosenza E. Incremental dynamic analysis of rigid blocks subjected to ground and floor motions and shake table protocol inputs. Bull N Z Soc Earthq Eng 2022;55. https://doi.org/10.5459/bnzsee.55.2.64-79.

[61] Prota A, Zito M, D'Angela D, Toscano G, Ceraldi C, Fiorillo A, Magliulo G. Preliminary results of shake table tests of a typical museum display case containing an art object. Adv Civ Eng 2022;2022:1–18. https://doi.org/10.1155/2022/3975958.
[62] Zito M, D'Angela D, Maddaloni G, Magliulo G. A shake table protocol for seismic assessment and qualification of acceleration-sensitive nonstructural elements. Comput Aided Civ Eng 2022:mice.12951. https://doi.org/10.1111/mice.12951.
[63] Zito M, Nascimbene R, Dubini P, D'Angela D, Magliulo G. Experimental seismic assessment of nonstructural elements: testing protocols and novel perspectives. Buildings 2022;12:1871. https://doi.org/10.3390/buildings12111871.
[64] Petrone C, Magliulo G, Manfredi G. Floor response spectra in RC frame structures designed according to Eurocode 8. Bull Earthq Eng 2016;14:747–67. https://doi.org/10.1007/s10518-015-9846-7.
[65] G.G. Deierlein, H. Krawinkler, C.A. Cornell, A framework for performance-based earthquake engineering., in: 2003.
[66] Gardoni P, Der Kiureghian A, Mosalam KM. PEER report 2002/13. Probabilistic models and fragility estimates for bridge components and systems. Berkeley, CA: Pacific Earthquake Engineering Research Center, University of California; 2002.
[67] FEMA. FEMA P-58-3: seismic performance assessment of buildings. Washington, DC: Performance Assessment Calculation Tool (PACT); 2012.
[68] Applied Technology Council. Recommendations for improved seismic performance of nonstructural components. Gaithersburg, MD: National Institute of Standards and Technology; 2018. https://doi.org/10.6028/NIST.GCR.18-917-43.
[69] Cremen G, Baker JW. Improving FEMA P-58 non-structural component fragility functions and loss predictions. Bull Earthq Eng 2019;17:1941–60. https://doi.org/10.1007/s10518-018-00535-7.
[70] American Society of Civil Engineers. Minimum design loads and associated criteria for buildings and other structures. 7th ed. Reston, VA: American Society of Civil Engineers; 2017. https://doi.org/10.1061/9780784414248.
[71] Liang H, Xie Q. Probabilistic seismic risk analysis of electrical substations considering equipment-to-equipment seismic failure correlations. Reliab Eng Syst Saf 2025;253:110588. https://doi.org/10.1016/j.ress.2024.110588.
[72] Porter K, Kennedy R, Bachman R. Creating fragility functions for performance-based earthquake engineering. Earthq Spectra 2007;23:471–89. https://doi.org/10.1193/1.2720892.
[73] ATC-58 Nonstructural Performance Products Team, ATC-58 Project Task Report Phase 2, Task 2.3 Engineering Demand Parameters for Nonstructural Components, Applied Technology Council, 201 Redwood Shores Parkway, Suite 240 Redwood City, California 94065, 2004. https://www.atcouncil.org/.
[74] Moehle J, Deierlein GG. A framework methodology for performance-based earthquake engineering. In: Proceedings of the 13th world conference on earthquake engineering; 2004. Paper No. 679.
[75] Di Sarno L, Magliulo G, D'Angela D, Cosenza E. Experimental assessment of the seismic performance of hospital cabinets using shake table testing. Earthq Eng Struct Dyn 2019;48:103–23. https://doi.org/10.1002/eqe.3127.
[76] Chen MC, Pantoli E, Wang X, Astroza R, Ebrahimian H, Hutchinson TC, Conte JP, Restrepo JI, Marin C, Walsh KD, Bachman RE, Hoehler MS, Englekirk R, Faghihi M. Full-scale structural and nonstructural building system performance during earthquakes: part I—Specimen description, test protocol, and structural response. Earthq Spectra 2016;32:737–70. https://doi.org/10.1193/012414EQS016M.
[77] Ministero delle Infrastrutture e dei Trasporti, Circolare 21 gennaio 2019, n. 7 C.S. LL.PP. Istruzioni per l'applicazione dell'«Aggiornamento delle "Norme tecniche per le costruzioni"» di cui al decreto ministeriale 17 gennaio 2018 (in Italian), (2019).
[78] Rodriguez D, Perrone D, Filiatrault A. Seismic demand on non-structural elements for quantifying seismic performance factors. Earthq Eng Struct Dyn 2022: eqe.3799. https://doi.org/10.1002/eqe.3799.
[79] Gabbianelli G, Perrone D, Brunesi E, Monteiro R. Seismic acceleration and displacement demand profiles of non-structural elements in hospital buildings. Buildings 2020;10:243. https://doi.org/10.3390/buildings10120243.
[80] International Code Council Evaluation Service (ICC-ES), AC156 Acceptance Criteria for the Seismic Qualification of Nonstructural Components, Brea, California, USA, 2020.
[81] International Organization for Standardization, ISO 13033:2013. Bases for design of structures—Loads, forces and other actions—Seismic actions on nonstructural components for building applications, (2013).
[82] CESMD, Center for Engineering Strong Motion Data, (2017). www.strongmotioncenter.org. Download on October 31st 2017.
[83] De Biasio M, Grange S, Dufour F, Allain F, Petre-Lazar I. Intensity measures for probabilistic assessment of non-structural components acceleration demand. Earthq Eng Struct Dyn 2015;44:2261–80. https://doi.org/10.1002/eqe.2582.
[84] Rota M, Zito M, Bianchi F, Dubini P. A new seismic classification procedure for nonstructural elements based on fragility curves. Buildings 2023;13:1017. https://doi.org/10.3390/buildings13041017.
[85] Mazza F. In-plane and out-of-plane nonlinear seismic response of masonry infills for hospitals retrofitted with hysteretic damped braces. Soil Dyn Earthq Eng 2021;148:106803. https://doi.org/10.1016/j.soildyn.2021.106803.
[86] Magliulo G, Petrone C, Capozzi V, Maddaloni G, Lopez P, Manfredi G. Seismic performance evaluation of plasterboard partitions via shake table tests. Bull Earthq Eng 2014;12:1657–77. https://doi.org/10.1007/s10518-013-9567-8.
[87] Ricci P, Di Domenico M, Verderame GM. Effects of the in-plane/out-of-plane interaction in URM infills on the seismic performance of RC buildings designed to Eurocodes. J Earthq Eng 2022;26:1595–629. https://doi.org/10.1080/13632469.2020.1733137.
[88] Karalar M, Çavuşlu M, Ozturk H, Mert N, Ahmad M, Sabri MMS. Assessing the 3D structural behavior of RC library buildings with/without non-structural elements considering shake table tests and 3D numerical analyses. Front Mater 2022;9:1066129. https://doi.org/10.3389/fmats.2022.1066129.
[89] Bakhtiary E, Gardoni P. Probabilistic seismic demand model and fragility estimates for rocking symmetric blocks. Eng Struct 2016;114:25–34. https://doi.org/10.1016/j.engstruct.2016.01.050.
[90] Oz B, Karalar M. A consensus-based Likert–LMBP model for evaluating the earthquake resistance of existing buildings. Appl Sci 2024;14:6492. https://doi.org/10.3390/app14156492.
[91] Perrone D, Aiello MA, Pecce M, Rossi F. Rapid visual screening for seismic evaluation of RC hospital buildings. Structures 2015;3:57–70. https://doi.org/10.1016/j.istruc.2015.03.002.
[92] Qin Z, Naser MZ. Machine learning and model driven bayesian uncertainty quantification in suspended nonstructural systems. Reliab Eng Syst Saf 2023;237:109392. https://doi.org/10.1016/j.ress.2023.109392.
[93] Cheng Q, Xie L, Wang Z, Liu Z, Lu X, Wang X. Multilevel assessment method for post-earthquake functionality of medical buildings considering component–department–floor interdependencies. Reliab Eng Syst Saf 2024;251:110379. https://doi.org/10.1016/j.ress.2024.110379.
[94] Structural Engineers Association Of California (SEAOC), Vision 2000 Report. Performance Based Seismic Engineering of Buildings, 1995.
[95] Bravo-Haro MA, Virreira JR, Elghazouli AY. Inelastic displacement ratios for non-structural components in steel framed structures under forward-directivity near-fault strong-ground motion. Bull Earthq Eng 2021;19:2185–211. https://doi.org/10.1007/s10518-021-01059-3.
[96] Linde SA, Konstantinidis D, Tait MJ. Rocking response of unanchored building contents considering horizontal and vertical excitation. J Struct Eng 2020;146:04020175. https://doi.org/10.1061/(ASCE)ST.1943-541X.0002735.
[97] Akkar S, Bommer JJ. Prediction of elastic displacement response spectra in Europe and the Middle East. Earthq Eng Struct Dyn 2007;36:1275–301. https://doi.org/10.1002/eqe.679.
[98] Fathali S, Lizundia B. Evaluation of current seismic design equations for nonstructural components in tall buildings using strong motion records. Struct Des Tall Build 2011;20:30–46. https://doi.org/10.1002/tal.736.
[99] Ishiyama Y. Motions of rigid bodies and criteria for overturning by earthquake excitations. Earthq Eng Struct Dyn 1982;10:635–50. https://doi.org/10.1002/eqe.4290100502.
[100] Makris N, Zhang J. Rocking response of anchored blocks under pulse-type motions. J Eng Mech 2001;127:484–93. https://doi.org/10.1061/(ASCE)0733-9399(2001)127:5(484).
[101] Di Egidio A, Alaggio R, Contento A, Tursini M, Loggia ED. Experimental characterization of the overturning of three-dimensional square based rigid block. Int J Non-Linear Mech 2015;69:137–45. https://doi.org/10.1016/j.ijnonlinmec.2014.12.003.
[102] The MathWorks Inc, Matlab 9.5., (2018).
[103] Applied Technology Council (ATC), ATC 63. Quantification of building seismic performance factors, California, 2008.
[104] Haselton CB, Deierlein GG. Assessing seismic collapse safety of modern reinforced concrete moment frame buildings. Stanford CA: The John A. Blume Earthquake Engineering Center, Department of Civil and Environmental Engineering, Stanford University; 2007.
[105] Deodatis G, Ellingwood BR, Frangopol DM. Safety, reliability, risk and life-cycle performance of structures and infrastructures. In: Proceedings of the 11th international conference on structural safety and reliability. CRC Press; 2014.
[106] Konstantinidis D, Makris N. Experimental and analytical studies on the seismic response of free standing and anchored laboratory equipment. Pacific Earthquake Engineering Research Center; 2005. https://doi.org/10.13140/rg.2.1.1469.2005. PEER 2005/07.
[107] McKenna F, Fenves GL, Scott MH. OpenSees: open system for earthquake engineering simulation. Berkeley, CA: Pacific Earthquake Engineering Research Center, University of California; 2000. Available at: http://opensees.berkeley.edu.
[108] Ibarra LF, Medina RA, Krawinkler H. Hysteretic models that incorporate strength and stiffness deterioration. Earthq Eng Struct Dyn 2005;34:1489–511. https://doi.org/10.1002/eqe.495.
[109] Lignos DG, Krawinkler H. Development and utilization of structural component databases for performance-based earthquake engineering. J Struct Eng 2013;139:1382–94. https://doi.org/10.1061/(ASCE)ST.1943-541X.0000646.
[110] Lignos DG, Krawinkler H. A steel database for component deterioration of tubular hollow square steel columns under varying axial load for collapse assessment of steel structures under earthquakes. In: Proceedings of the 7th international conference on urban earthquake engineering (7CUEE) & 5th international conference on earthquake engineering (5ICEE); 2010.